NAVAL POSTGRADUATE SCHOOL
Monterey, California

THESIS

THE EFFECT OF THERMOMECHANICAL PROCESSING ON THE TENSILE PROPERTIES AND MICROSTRUCTURE OF A 6061 AL-AL_2O_3 METAL MATRIX COMPOSITE

by

Michael A. Ballou

December 1995

Thesis Advisor: Terry R.McNelley

Approved for public release; distribution is unlimited.

DISCLAIMER NOTICE

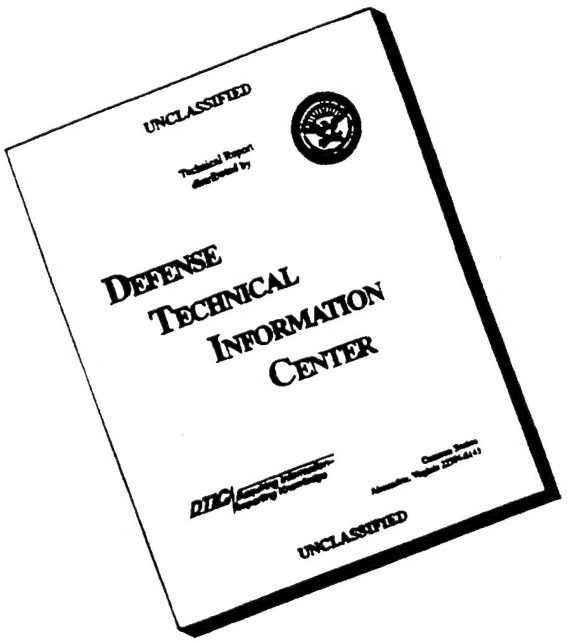

THIS DOCUMENT IS BEST QUALITY AVAILABLE. THE COPY FURNISHED TO DTIC CONTAINED A SIGNIFICANT NUMBER OF PAGES WHICH DO NOT REPRODUCE LEGIBLY.

REPORT DOCUMENTATION PAGE

Form Approved OMB No. 0704

1. AGENCY USE ONLY *(Leave blank)*	2. REPORT DATE	3. REPORT TYPE AND DATES COVERED
	December 1995	Engineer's Thesis

4. TITLE AND SUBTITLE **THE EFFECT OF THERMOMECHANICAL PROCESSING ON THE TENSILE PROPERTIES AND MICROSTRUCTURE OF A 6061 Al_2O_3 METAL MATRIX COMPOSITE**

5. FUNDING NUMBERS

6. AUTHOR(S) Ballou, Michael A.

7. PERFORMING ORGANIZATION NAME(S) AND ADDRESS(ES)
Naval Postgraduate School
Monterey CA 93943-5000

8. PERFORMING ORGANIZATION REPORT NUMBER

9. SPONSORING/MONITORING AGENCY NAME(S) AND ADDRESS(ES)

10. SPONSORING/MONITORING AGENCY REPORT NUMBER

11. SUPPLEMENTARY NOTES The views expressed in this thesis are those of the author and do not reflect the official policy or position of the Department of Defense or the U.S. Government.

12a. DISTRIBUTION/AVAILABILITY STATEMENT
Approved for public release; distribution unlimited

12b. DISTRIBUTION CODE

13. ABSTRACT *(maximum 200 words)* This work includes a comprehensive analysis of the effect of thermomechanical processing (TMP) history on the microstructure and properties of 10 and 20 volume percent 6061 Al-Al_2O_3 discontinuous metal matrix composites (MMCs). Materials in which cold drawing operations were included in the TMP demonstrated increased ductilities for a given strength level when compared to samples which were processed by hot extrusion only. Microstructural analysis provided clear evidence of the absence of damage to reinforcing particles during TMP and of load transfer to these particles during subsequent straining. Failure during tension testing resulted from the ductile tearing of the matrix as voids, initiated by the cracking of reinforcement particles, joined together. A distinct microstructural difference related to processing history was the development of a strongly fibered particle distribution in materials experiencing low temperature drawing operations. In order to conduct an analysis of the mechanisms by which the particles are redistributed and reoriented during processing, a channel compression die was constructed which allowed processing to be simulated by compressive straining on a mechanical testing machine. This allowed careful control of the processing parameters. An analysis of the effects of processing temperature on particle redistribution and reorientation was conducted.

14. SUBJECT TERMS Composite Materials, Metal Matrix Composites (MMCs), Particle Stimulated Nucleation (PSN), Recrystallization, Plastic Deformation, Dislocations, Grain Boundary Sliding

15. NUMBER OF PAGES
82

16. PRICE CODE

17. SECURITY CLASSIFICATION OF REPORT	18. SECURITY CLASSIFICATION OF THIS PAGE	19. SECURITY CLASSIFICATION OF ABSTRACT	20. LIMITATION OF ABSTRACT
Unclassified	Unclassified	Unclassified	UL

NSN 7540-01-280-5500

Standard Form 298 (Rev. 2-89)
Prescribed by ANSI Std. 239-18

Approved for public release: distribution is unlimited.

THE EFFECT OF THERMOMECHANICAL PROCESSING ON THE TENSILE PROPERTIES AND MICROSTRUCTURE OF A 6061 Al-Al_2O_3 METAL MATRIX COMPOSITE

Michael A. Ballou
Lieutenant, United States Navy
B.S., United States Naval Academy, 1989

Submitted in partial fulfillment
of the requirements for the degree of

MECHANICAL ENGINEER

from the

NAVAL POSTGRADUATE SCHOOL
December 1995

Author: Michael A. Ballou
Michael A.Ballou

Approved by: T. R. McNelley
T. R. McNelley, Thesis Advisor

Matthew Kelleher
Matthew D. Kelleher, Chairman
Department of Mechanical Engineering

ABSTRACT

This work includes a comprehensive analysis of the effect of thermomechanical processing (TMP) history on the microstructure and properties of 10 and 20 volume percent 6061 Al-Al_2O_3 discontinuous metal matrix composites (MMCs). Materials in which cold drawing and annealing operations were included in the TMP demonstrated increased ductilities for a given strength level when compared to materials which were processed by hot extrusion only. Microstructural analysis provided clear evidence of the absence of damage to reinforcing particles during TMP and of load transfer to these particles during subsequent straining. Failure during tension testing resulted from the ductile tearing of the matrix as voids, initiated by the cracking of reinforcement particles, joined together. A distinct microstructural difference related to processing history was the development of a strongly fibered particle distribution in materials experiencing low temperature drawing operations. In order to conduct an analysis of the mechanisms by which the particles are redistributed and reoriented during processing, a channel compression die was constructed which allowed processing to be simulated by compressive straining on a mechanical testing machine. This allowed careful control of the processing parameters. An analysis of the effects of processing temperature on particle redistribution and reorientation was conducted.

TABLE OF CONTENTS

LIST OF FIGURES

ACKNOWLEDGMENTS

I would like to thank DURALCAN-USA for providing the materials for this study, as well as the Army Research Laboratory/Army Research Office for financial support of this research.

I would also like to thank my advisor, Dr. Terry R. McNelley for his guidance and encouragement during the course of this thesis work. His knowledge of the subject was invaluable and his enthusiasm made this difficult project truly enjoyable. I would also like to thank Douglas Shelton and Richard Hashimoto for their many hours of assistance with laboratory equipment. Finally, my sincerest thanks to my wife Sherry without whose support and encouragement this work would not have been possible.

I. INTRODUCTION

Composite materials have seen steady growth in their use, particularly in the defense industries. The improved physical and mechanical properties of composites when compared to unreinforced materials make their use desirable, but the expense of incorporation of these materials into engineering systems has been a limiting factor in their usage. Metal Matrix Composites (MMCs) are a growing area within the composite materials field. Aluminum alloys reinforced with particles of either Al_2O_3 or SiC have been studied extensively. These materials have been produced primarily by powder metallurgy methods in the past, but DURALCAN-USA of San Diego, CA has pioneered production by ingot metallurgy methods. These methods offer promise for high volume, low cost production of MMCs in the future [Ref. 1].

Other than by cost, widespread usage of particle-reinforced MMCs has been restricted by low ductilities and poor fracture toughnesses compared to traditional unreinforced engineering materials. If these shortcomings can be overcome, the beneficial properties of these materials, namely higher strength, higher stiffness and better wear resistance than the unreinforced material, could be exploited in many engineering applications. Previous work [Refs. 2-9] has demonstrated that appropriate Thermomechanical Processing (TMP) can be used to improve ductility in these materials with little or no loss in strength. In this study, the tensile behavior of both Al 6061-10 v/o Al_2O_3 MMC and Al 6061-20 v/o Al_2O_3 MMC was studied. The behavior for different

TMP conditions and different aging conditions was considered. Both tensile properties and modes of failure were investigated.

One microstructural characteristic of particular interest in particle reinforced composites is the homogeneity of the particle distribution. Manfredi, in a study of characterization of particle distributions by computer simulation [Ref. 10], concluded that the human eye is the most effective differentiator between random and non-random distributions. Although it may be difficult to characterize, the homogeneity of the particle distribution is clearly important to mechanical properties in these materials; preferential void nucleation during tension is frequently observed in regions of high volume fraction [Ref. 11]. In production of these materials, large processing strains are used to homogenize the particle distribution. Despite the acceptance of this practice, the mechanisms by which particles are redistributed during straining have not been studied. The second goal of this study was to observe the microstructure of an Al 6061-10 v/o Al_2O_3 MMC at incremental stages of both hot and cold TMP routines in an effort to understand the mechanisms involved in particle redistribution.

II. BACKGROUND

The field of composite materials is not a new one. Many common engineering materials are, strictly speaking, composites. Carbon black in rubber, cement mixed with sand and glass fibers in resin are examples of widely used composite materials [Ref. 12]. Wood, bone and other naturally occurring materials can also be characterized as composites. A convenient definition of a composite material is one that 1), is manufactured; 2), consists of two or more physically and/or chemically distinct, suitably arranged or distributed phases with an interface separating them; and 3), has characteristics that are not displayed by any of the components in isolation [Ref. 12]. Engineered composite materials are composites that are designed to achieve specific material property combinations. Designing an optimum material to meet engineering requirements promises much more efficient products than simply designing components to conform to the limitations of conventional engineering materials. In fact, in the aerospace industry the necessity of efficient design has made the use of engineered materials the norm [Ref 13].

Composite materials are sometimes classified by the type of reinforcement used. Continuous-fiber reinforced composites offer optimum transfer of load to the reinforcing fibers, but properties are anisotropic. This problem is generally alleviated by constructing a laminate of plies with different fiber orientations. Discontinuously reinforced composites include materials reinforced with particles and whiskers. Although less load can be transferred to the reinforcement in these materials, properties are fairly isotropic. Unlike

continuously reinforced composites, matrix strength contributes substantially to the strength of a discontinuously reinforced composite [Ref. 14].

Another method of classifying composites is by matrix material. The three classifications of composites are Polymer Matrix Composites (PMCs), Ceramic Matrix Composites (CMCs) and Metal Matrix Composites (MMCs). PMCs reinforced with glass fibers, as well as more advanced fibers (Carbon, Kevlar and Boron) have gained wide acceptance [Ref. 12]. Both continuous and discontinuous fibers have been used in these materials. In this case, the reinforcement is used primarily to increase the strength of the composite. In CMCs, the matrix material is already extremely strong. Fibers are incorporated in these materials to increase the toughness of the ceramic, allowing its high temperature strength and environmental resistance to be utilized but reducing the risk of catastrophic failure [Ref. 12]. MMCs, like PMCs, gain strength from the reinforcement. Unlike PMCs, MMCs have a formable matrix. This fact makes the integration of component design and material specification less crucial in MMCs than in PMCs [Ref. 14].

The first modern MMCs were dispersion hardened metal systems [Ref. 14]. Extensive research was conducted on consolidated mixtures of Al and Al_2O_3 powder during the 1950s and 1960s [Ref. 15]. In developing these materials, very small particles ($<1\,\mu m$) were used. The strengthening mechanism in these materials was anticipated to be the same as that in precipitation hardened materials, namely Orowan strengthening. The basis of this mechanism is to impede the motion of dislocations through the usage of either fine oxide particles or non-shearable precipitates [Ref. 14]. Although precipitation hardened systems offer the advantage of easily achieved fine distributions, dispersion

hardened systems are superior at elevated temperatures because of the high thermal stability of the oxide particles [Ref 14]. More recent developments in MMCs have involved the use of much larger reinforcement particles (1-100 μm). These particles are too large for substantial strengthening by the Orowan mechanism. Instead, strengthening occurs through load transfer from the matrix to the reinforcement by shear at the interface. In the past, these composites have been manufactured almost exclusively by powder metallurgy methods. These methods are fairly expensive and are not practical for large volume production. Ingot metallurgy methods offer promise for low-cost, high-volume production of these materials. Complete wetting of the reinforcement particles during mixing is essential to ensure good interfacial bonding and to avoid porosity. Particle surface treatments and appropriate particle size must be exploited to achieve good wetting during mixing. DURALCAN-USA of San Diego, CA has developed a proprietary ingot metallurgy process for production of particle reinforced MMCs. This process involves particle pretreatment, stirring particles into the molten matrix, and producing either chill casts for extrusion or rolling slabs. Composites which have been produced by this method have used primarily Al 6061 alloy matrix material, although both 2000 and 7000 series aluminum alloys have been used for higher strength applications. Particle sizes for each composite are tailored to ensure good wetting. Larger particle sizes are used for larger volume fraction composites to avoid increasing the surface area to volume ratio (particle size for the Al 6061-10 v/o Al_2O_3 MMC are nominally 12.5 μm while the Al 6061-20 v/o Al_2O_3 MMC particle size is nominally 19.0 μm). MMCs containing either SiC or Al_2O_3 particles have been produced by this method.

Applications for these MMCs are varied. DURALCAN has primarily marketed wrought products. Some of these include tubing for bicycle frames and driveshafts, and forging stock for connecting rods. The availability of low cost MMCs has stimulated research efforts by the Army Research Laboratory to exploit their potential use in Army applications [Ref. 16]. One possible application would be materials for a lightweight armored vehicle. Growth in usage of these materials has been slower than was anticipated in the 1980s. Low ductility (<10% elongation in 10 and 20 volume percent materials) and poor fracture toughness (K_{IC} values < 15 $MPam^{1/2}$) have restricted their use.

Previous work in this laboratory [Refs. 2-9] adapted TMP schedules developed for use with superplastic Al-Mg alloys [Refs. 17-24] for use with either rolled or extruded Al 6061-10 v/o Al_2O_3 MMCs and Al 6061-20 v/o Al_2O_3 MMCs. The goal of these TMP schedules was to enhance the ductility in these materials. These studies concluded that ductility could be enhanced in these materials through control of parameters during rolling. Hoyt applied hot forging followed by rolling and intermediate annealing stages to cast billets of these materials [Ref. 1]. He was able to achieve homogeneous particle distributions and matrix grain refinement through this TMP. Enhanced ductility was reported in MMCs processed to sufficient strain and solution heat treated at temperatures low enough to maintain the matrix grain refinement. Longenecker developed a similar TMP schedule that made use of a combination of hot extrusions and cold drawing/intermediate annealing operations [Ref. 25].

The first portion of this work investigated the microstructure, tensile properties and fracture mechanisms in both the Al 6061-10 v/o Al_2O_3 MMCs and Al 6061-20 v/o

Al_2O_3 MMCs processed in accordance with Longenecker's TMP schedule. Both underaged and peak aged materials were investigated.

The mechanical properties of particle reinforced MMCs have been linked to the uniformity of the particle distribution [Refs. 2, 9, 26 and 27]. Previous work in this laboratory [Ref. 25] has shown that true processing strains on the order of 4.0 are necessary to achieve a homogeneous particle distribution in these materials. The effect of processing temperature on the redistribution of the particles has not been studied. In fact, the mechanisms by which particles are redistributed in these materials have not been determined. The second portion of this study was an investigation of the mechanisms by which particles are redistributed in these materials during processing. The effect of processing temperature on particle redistribution was also investigated.

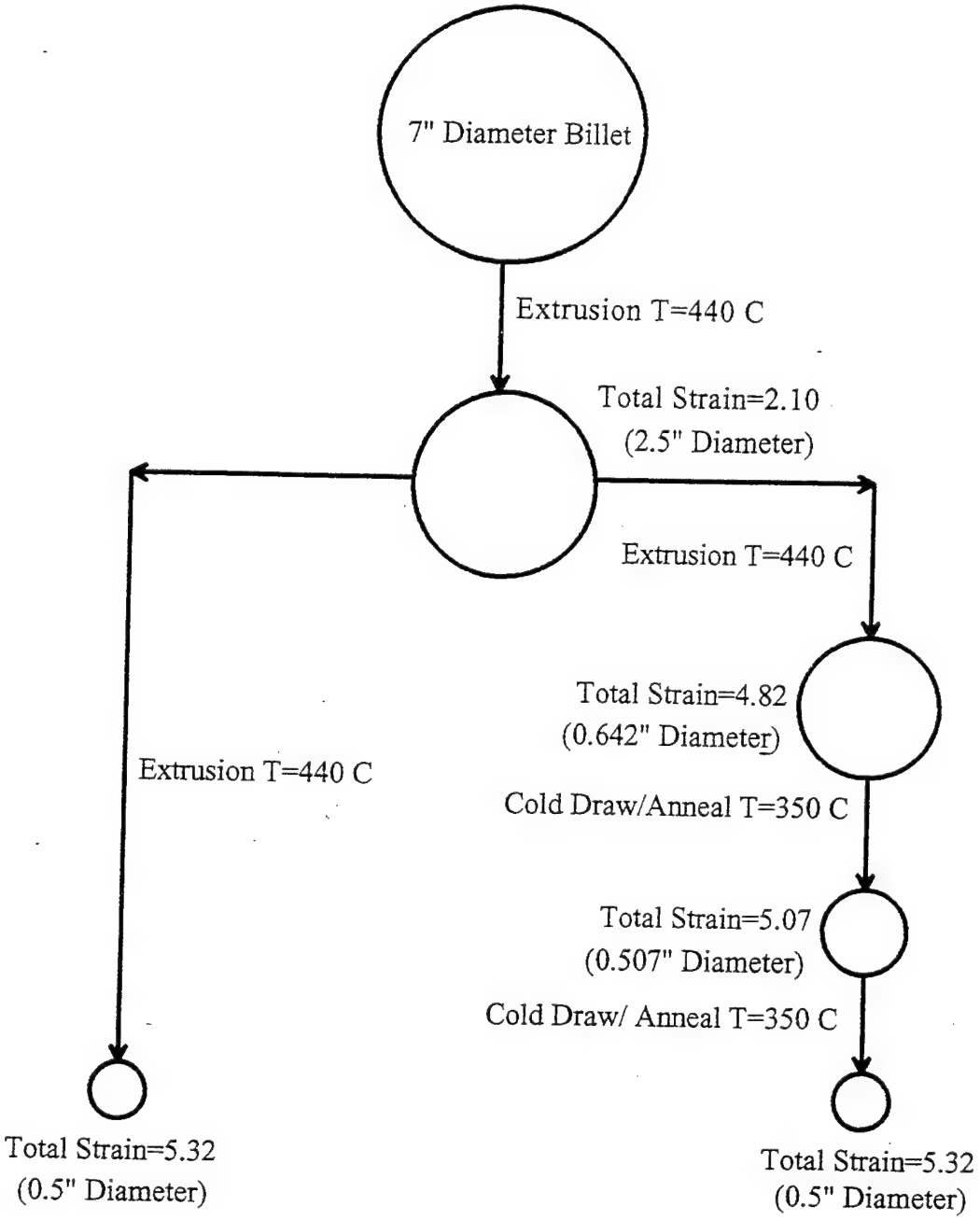

Figure 1: **Processing Schedule Used for Both the Al 6061-10 v/o Al_2O_3 MMCs and Al 6061-20 v/o Al_2O_3 MMCs.**

testing. The buttonhead type tensile specimen designed and validated by Longenecker was used; the gage section was 3.10 cm (1.22 in) in length and 0.51 cm (0.20 in) in diameter in this design [Ref. 25].

Solution heat treating of as-machined tensile specimens was carried out in a Lindberg type 51222 furnace. All samples were solution heat treated at a temperature of 530°C for 70 minutes. Aging was carried out in a Blue-M oven, Model OV-490A-3, at 160°C. Materials with no aging, as well as with aging times of one, four and sixteen hours were prepared. Both solutionizing and aging were carried out in accordance with procedures described in the Metals Handbook [Ref. 29].

Tensile testing of materials was conducted in previous work [Ref. 28] utilizing an Instron Model 4507 testing machine. Data were collected and processed on a Zenith 386 personal computer using Instron's Series IX Automated Testing System software.

Fracture surfaces of all samples were investigated in a Cambridge Stereoscan 200 Scanning Electron Microscope (SEM). To avoid charging of the Al_2O_3 particles, the fracture surfaces were first coated with carbon using a Fullam EFFA Mk11 Carbon Coater. All SEM images were obtained in the secondary electron mode with an accelerating voltage of 25 Kev. Images were recorded using Polaroid Type T-55 positive/negative film.

Following deformation to failure, tensile specimens were sectioned longitudinally along the gage length using an Isomet 11-1180 low speed saw with a diamond impregnated blade. Specimens were then cold mounted such that the profile of the fracture surface could be observed. A hole was drilled through the side of each cold

mount and a wood screw was threaded through the cold mount to establish electrical contact with the specimen. This was most easily accomplished before the cold-mount material had fully set. The hole was drilled in the side such that the electrical contact would not be immersed in the electrolyte during subsequent anodizing.

Samples were ground using waterproof carbide paper on a Knuth Rotor Grinder with water for lubrication. Polishing was carried out using diamond spray on Metadi Extender microcloth. Final polishing was with 0.05 μm colloidal silica. The detailed grinding and polishing schedule developed previously by Hoyt [Ref. 1] was followed closely.

Optical microscopy was carried out on a Zeiss Xenophot optical microscope. 35mm photographs were taken with Kodak TMAX100 black and white film. In order to investigate grain structure, the samples were anodized in Barkers Reagent using procedures delineated by Hoyt [Ref. 1]. Anodized samples were then investigated on a Zeiss ICM-405 optical microscope under crossed polars. This particular microscope was superior for obtaining contrast for black and white prints. Photographs were taken with Polaroid Type T-55 positive/negative film.

C. RESULTS/DISCUSSION

Results of the tensile testing are depicted in Appendices A through D. Figures 2 and 3 summarize the results for the Al 6061-10 v/o Al_2O_3 MMC and the Al 6061-20 v/o Al_2O_3 MMC. In both cases, it is clear that the materials which were processed using cold

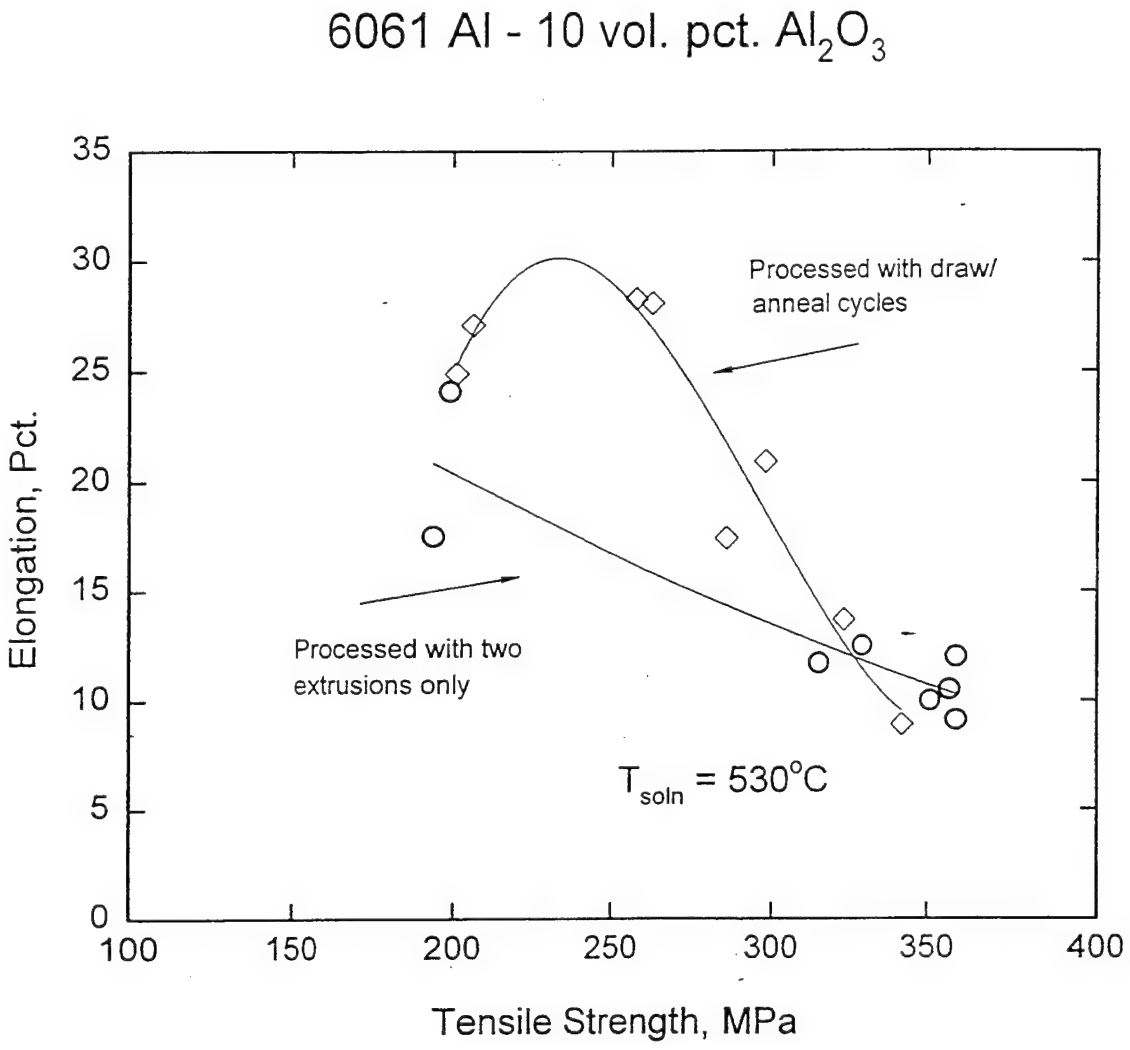

Figure 2: **Percent Elongation as a Function of Tensile Strength for the Al 6061-10 v/o Al_2O_3 MMC.**

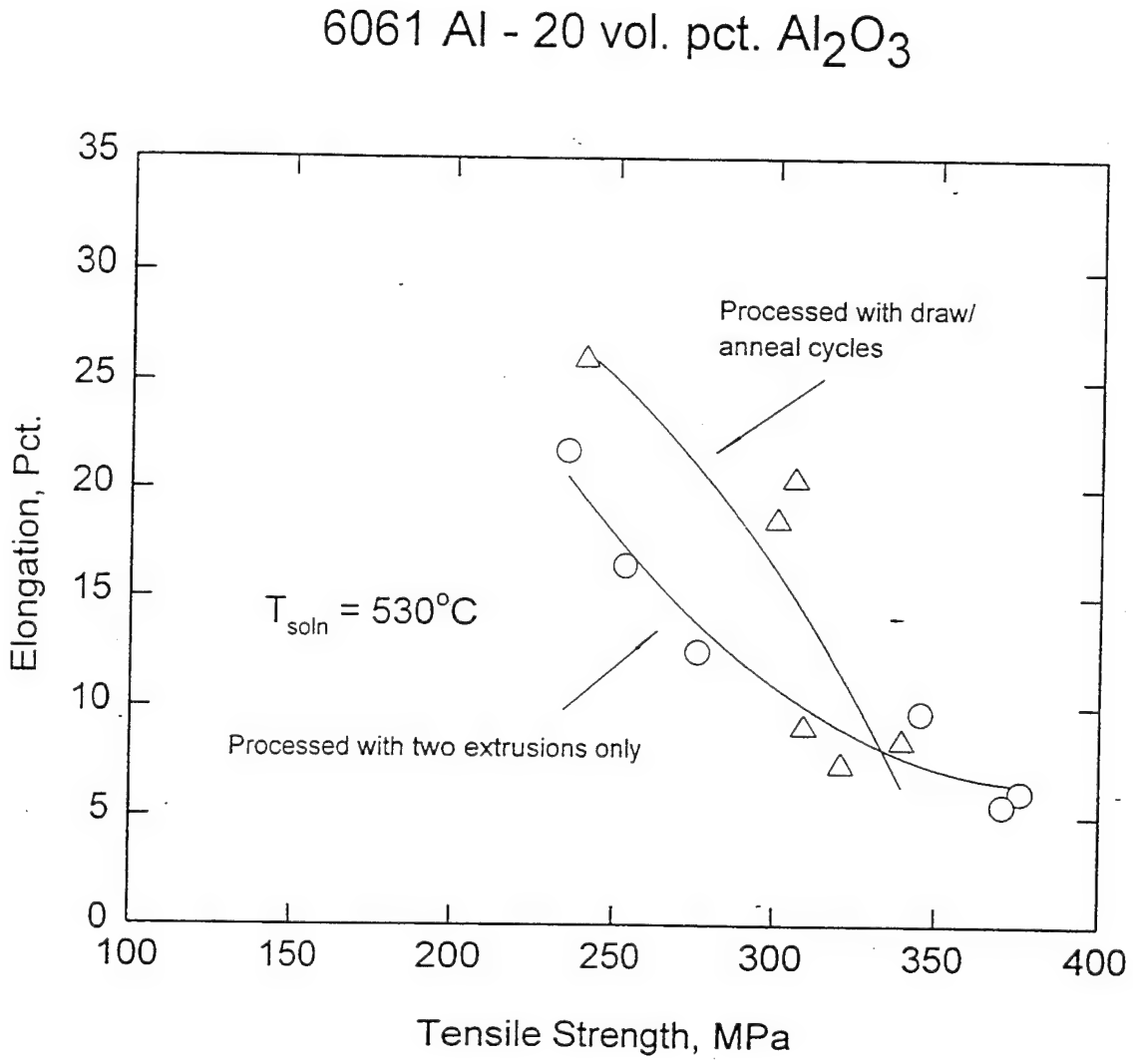

Figure 3: **Percent Elongation as a Function of Tensile Strength for the Al 6061-20 v/o Al_2O_3 MMC.**

drawing and intermediate annealing operations exhibited an increase in ductility in the underaged state. The ductilities of these materials, as measured by percent elongation, are well in excess of the corresponding ductilities of the materials which were processed only by extrusion to the same total strain. Since the poor ductility of particulate reinforced MMCs is acknowledged to be a significant concern, this observation is extremely noteworthy.

The effect of the TMP history on the microstructure of the material was investigated in an effort to understand the mechanism by which the materials which were cold drawn and annealed had achieved enhanced ductility. In the initial phase of this analysis, the buttonhead ends of the samples were used. This was done to ensure that only the effects of the processing and not those of the tensile testing were observed.

Figure 4 shows the particle distribution in an Al 6061-10 v/o Al_2O_3 MMC which has been extruded only, and Figure 5 shows the distribution in the same material when it has also seen cold drawing and annealing in the later stages of deformation. The particles in the material which has been processed only by extrusion are well distributed. However, the particles in the material which has been extruded and then cold drawn and annealed to the final processing strain are not as well distributed. Instead, the distribution of these particles is more highly banded in the drawing direction. In this case, nonuniform distribution in the form of banding of the reinforcement particles does not have a negative impact on the tensile properties. However, since tensile testing was only carried out along the extrusion axis, the effect of this mechanical fibering on the transverse properties is not known. It is likely, however, that the properties of this MMC will be anisotropic.

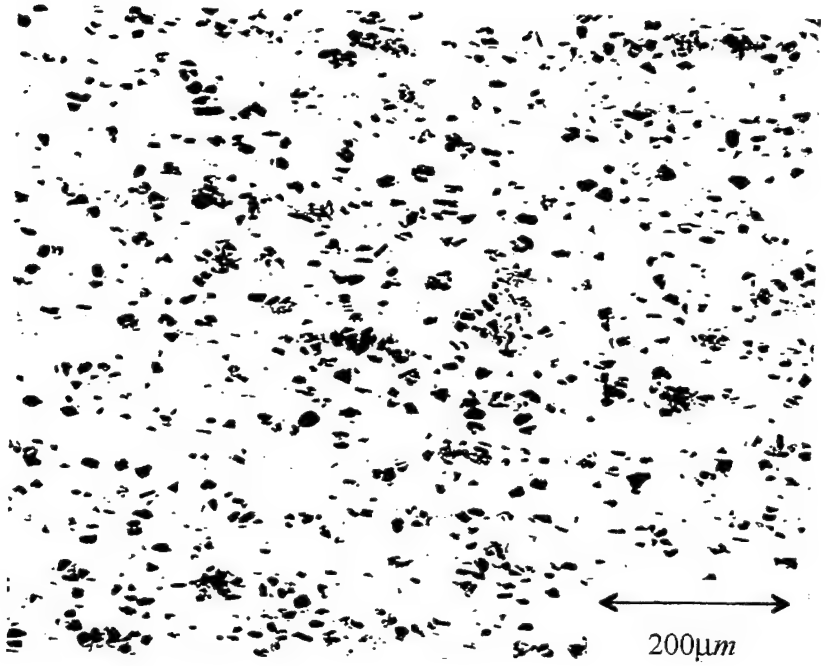

Figure 4: **Optical Micrograph of the Al 6061-10 v/o Al_2O_3 MMC Which Has Been Processed Only by Extrusions.**

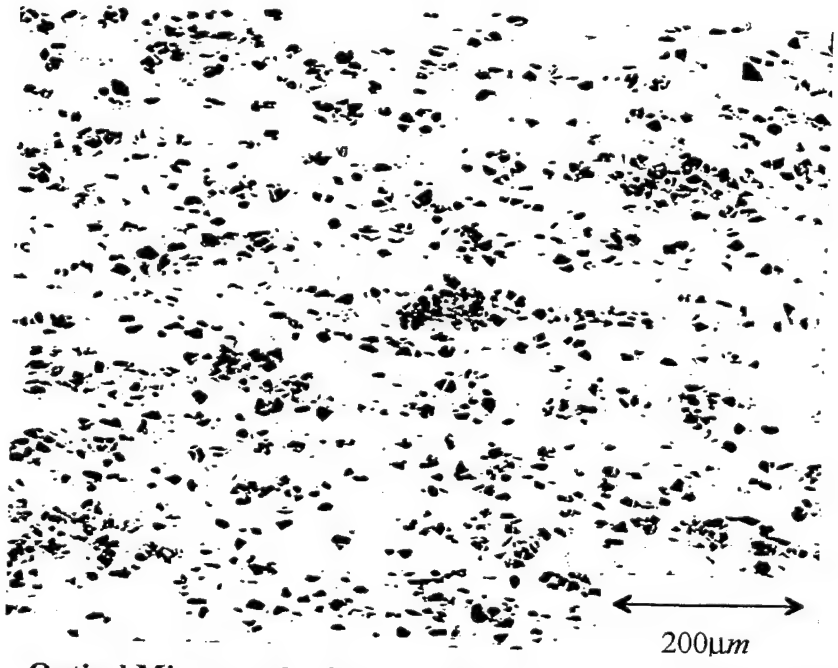

Figure 5: **Optical Micrograph of the Al 6061-10 v/o Al_2O_3 MMC Which Has Been Processed by Extrusions and Draw/Anneal Cycles.**

Figure 6 illustrates the grain structure of an Al 6061-10 v/o Al_2O_3 MMC which was processed only by extrusions while Figure 7 shows the grain structure of the same material which was processed by both extrusions and cold drawing and annealing operations. There is no apparent difference in the grain structure.

Figures 8 shows corresponding data on the particle distribution in an Al 6061-20 v/o Al_2O_3 MMC which has been extruded only, and Figure 9 those which have also seen cold drawing and annealing in the later stages of deformation. For this higher volume fraction material, the particle distribution is very homogeneous for both processing routes. This is in contrast with the observation of more severe banding in the cold-drawn Al 6061-10 v/o Al_2O_3 MMC. Such a difference in behavior during processing may reflect volume fraction or particle size effects, or both. Figures 10 and 11 demonstrate that there is no difference in grain structure for the 6061-20 v/o Al_2O_3 MMC between the two processing routines. Finally, the optical microscopy of these materials discussed earlier (Figures 4, 5, 8 and 9) shows no evidence of significant particle cracking in either material for either processing route. In fact, previous work [Ref. 25] had shown no significant change in mean aspect ratio, mean maximum particle diameter or mean particle diameter in materials processed by these TMPs.

Subsequently, the gage sections of the tensile samples were investigated using both optical microscopy and polarized light optical microscopy. Optical microscopy of all gage section samples (Figures 12-19) clearly shows numerous cracked particles. These micrographs were taken along the centerline of each sample at a distance of two to five millimeters from the fracture surface. The particle cracks are almost exclusively

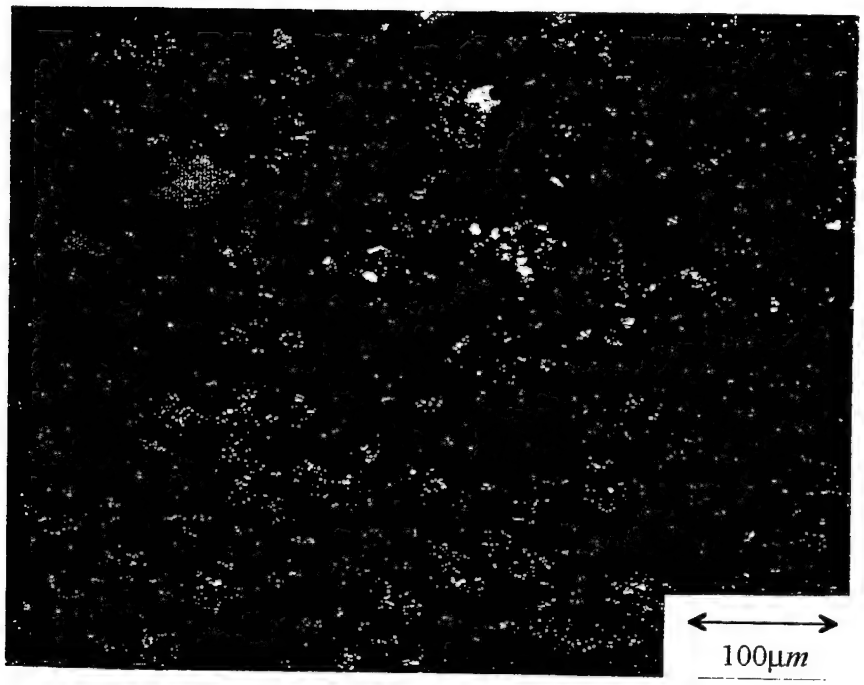

Figure 6: **Polarized Light Optical Micrograph of the Al 6061-10 v/o Al_2O_3 MMC Which Has Been Processed Only by Extrusions.**

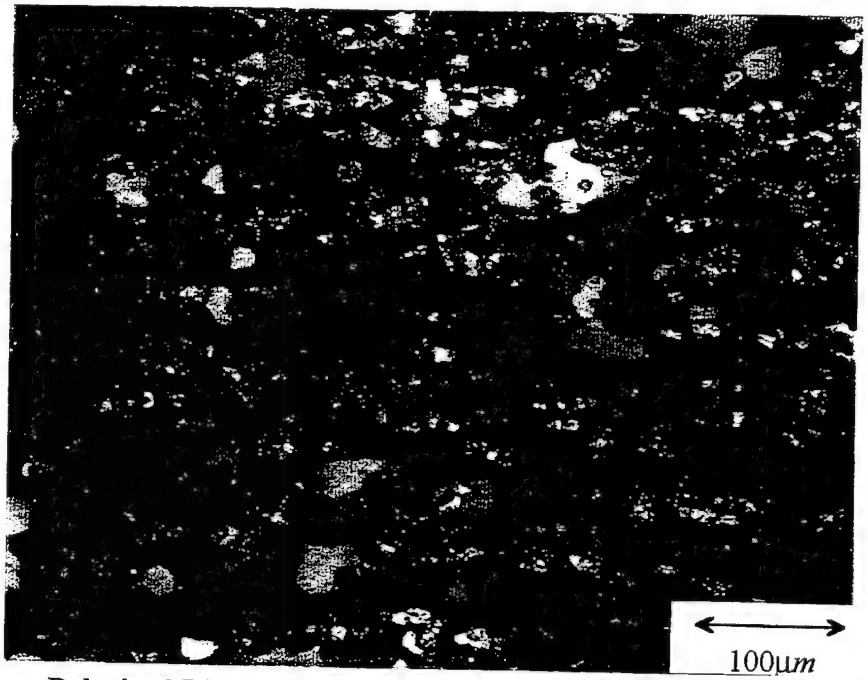

Figure 7: **Polarized Light Optical Micrograph of the Al 6061-10 v/o Al_2O_3 MMC Which Has Been Processed by Extrusions and Draw/Anneal Cycles.**

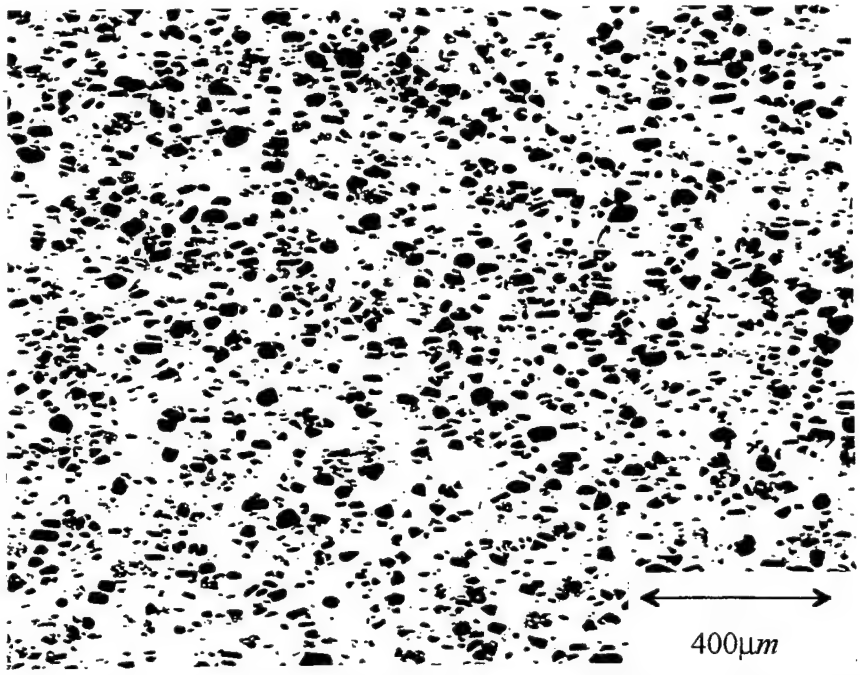

Figure 8: **Optical Micrograph of the Al 6061-20 v/o Al_2O_3 MMC Which Has Been Processed Only By Extrusions.**

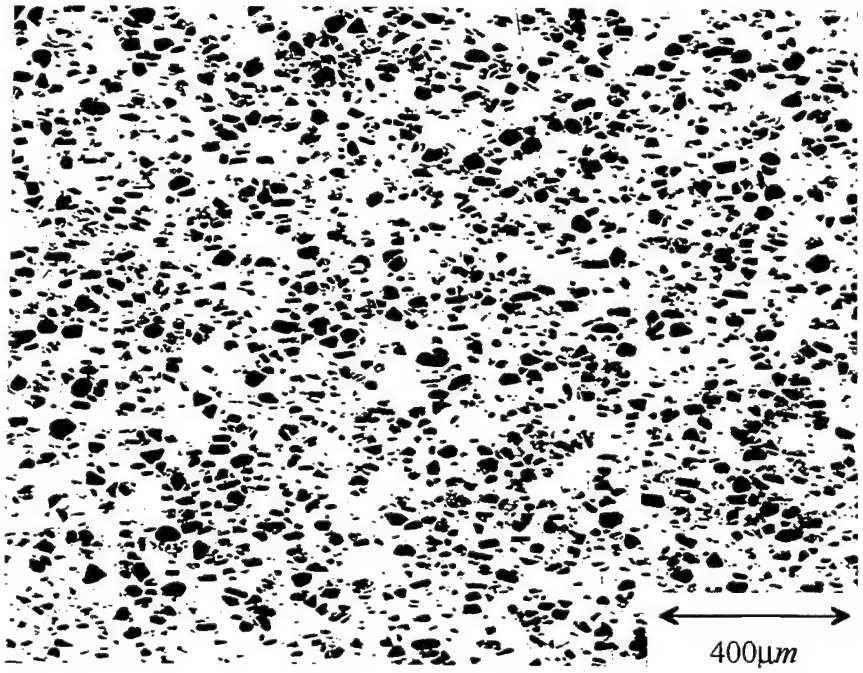

Figure 9: **Optical Micrograph of the Al 6061-20 v/o Al_2O_3 MMC Which Has Been Processed by Extrusions and Draw/Anneal Cycles.**

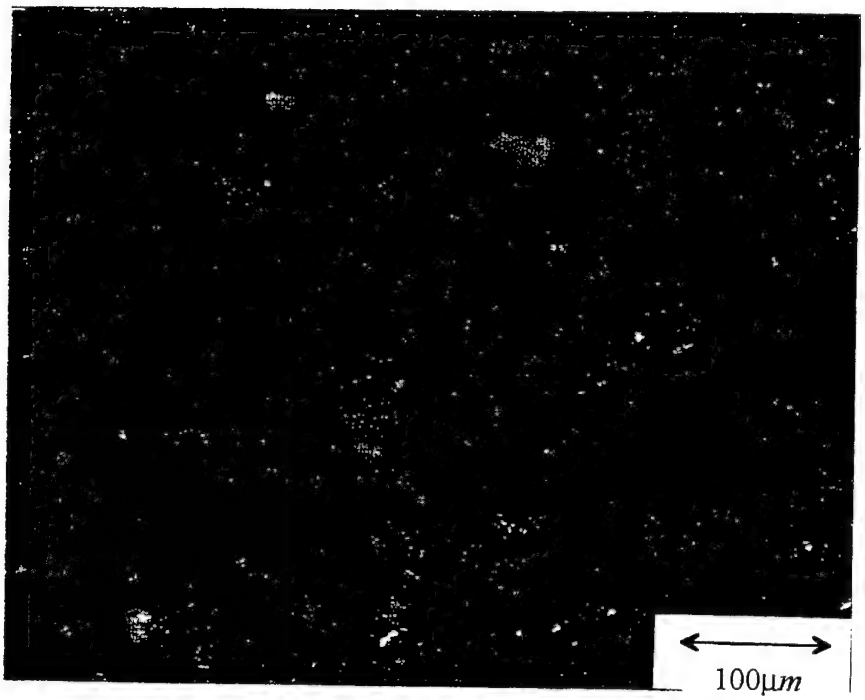

Figure 10: **Polarized Light Optical Micrograph of the Al 6061-20 v/o Al_2O_3 MMC Which Has Been Processed Only By Extrusions.**

Figure 11: **Polarized Light Optical Micrograph of the Al 6061-20 v/o Al_2O_3 MMC Which Has Been Processed by Extrusions and Draw/Anneal Cycles .**

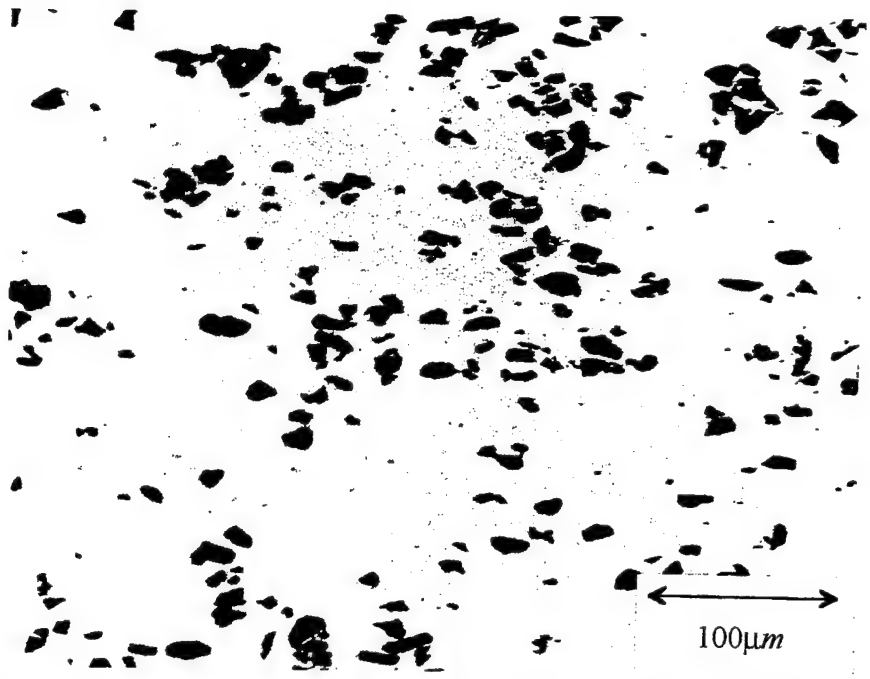

Figure 12: **Optical Micrograph of the Al 6061-10 v/o Al_2O_3 MMC Which Has Been Processed Only by Extrusions (Underaged Condition, Gage Section).**

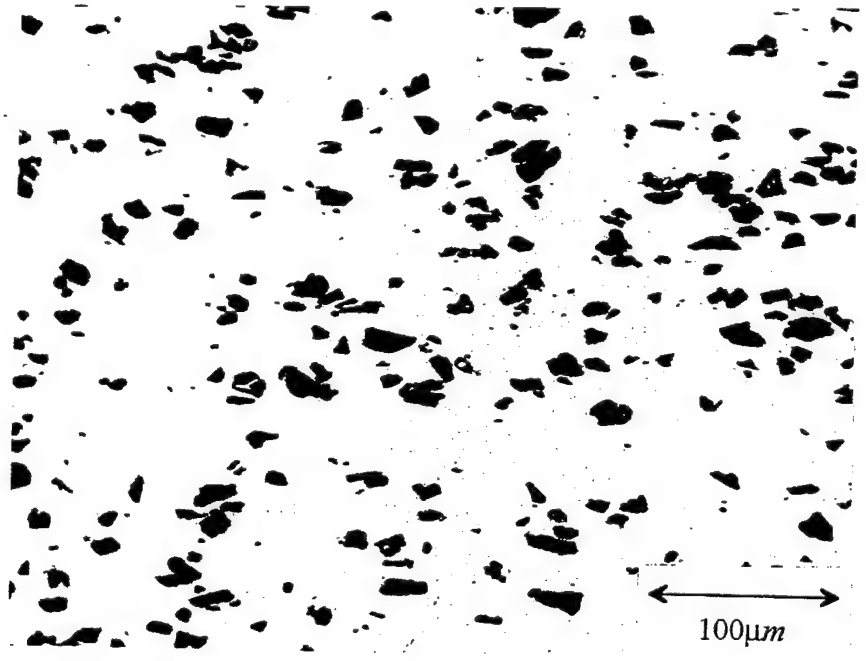

Figure 13: **Optical Micrograph of the Al 6061-10 v/o Al_2O_3 MMC Which Has Been Processed Only by Extrusions (Peak Aged Condition, Gage Section).**

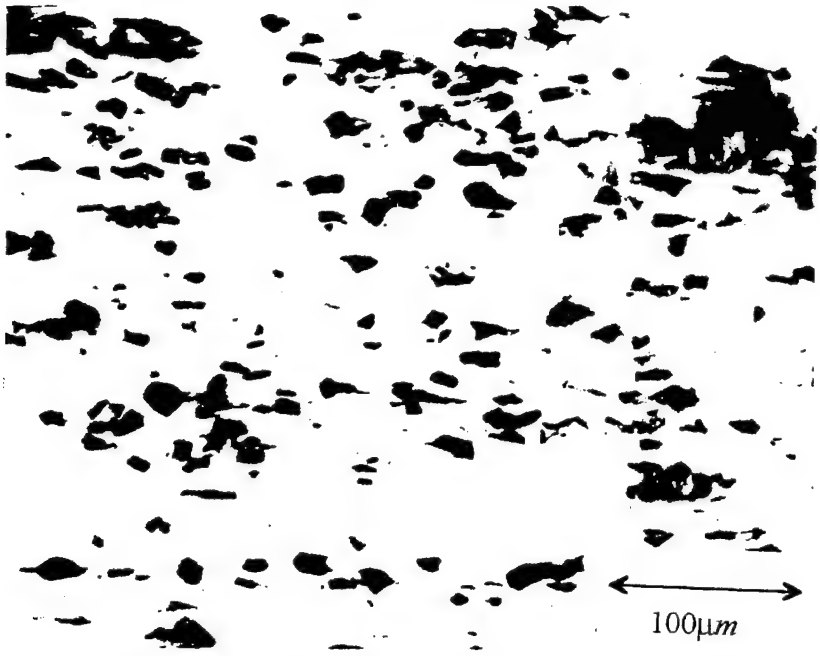

Figure 14: **Optical Micrograph of the Al 6061-10 v/o Al_2O_3 MMC Which Has Been Processed by Extrusions and Draw/Anneal Cycles (Underaged Condition, Gage Section).**

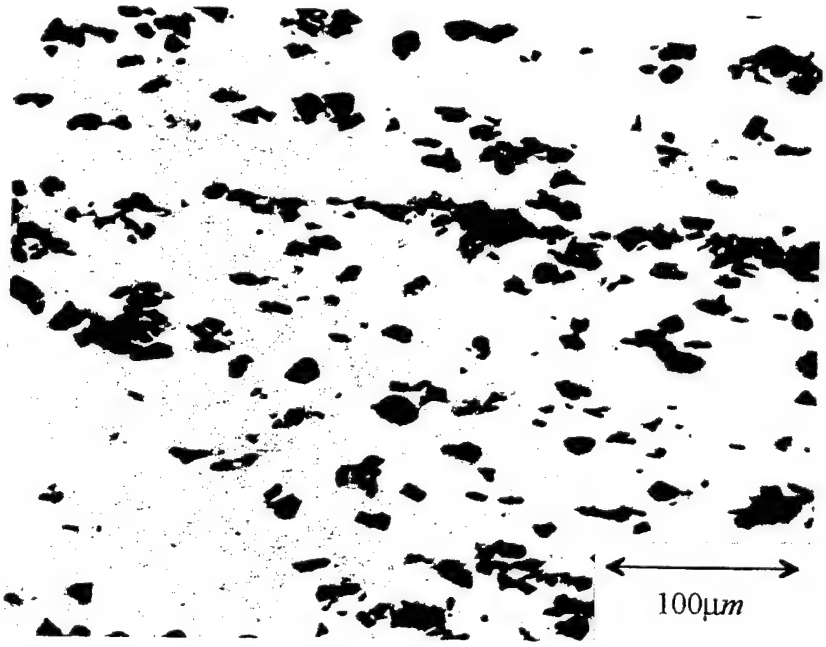

Figure 15: **Optical Micrograph of the Al 6061-10 v/o Al_2O_3 MMC Which Has Been Processed by Extrusions and Draw/Anneal Cycles (Peak Aged Condition, Gage Section).**

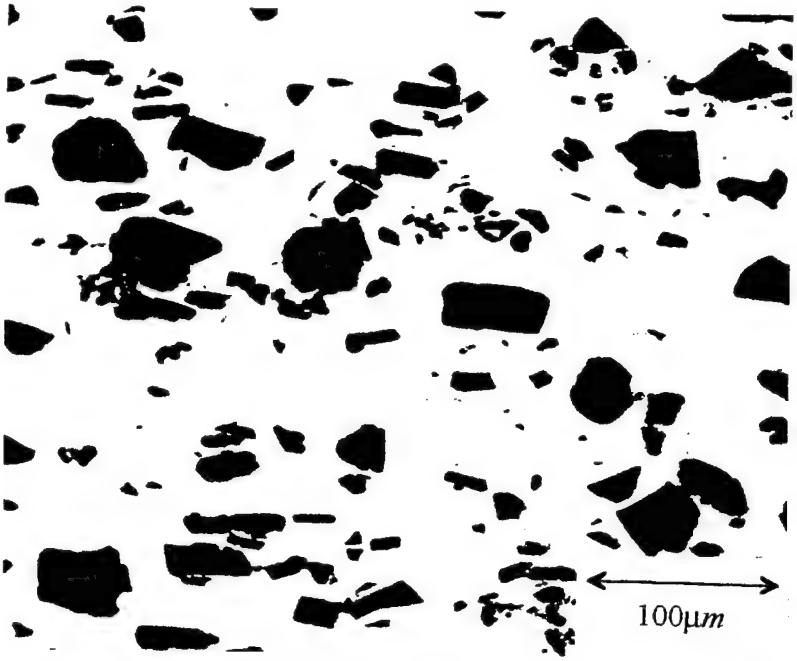

Figure 16: **Optical Micrograph of the Al 6061-20 v/o Al_2O_3 MMC Which Has Been Processed Only by Extrusions (Underaged Condition, Gage Section).**

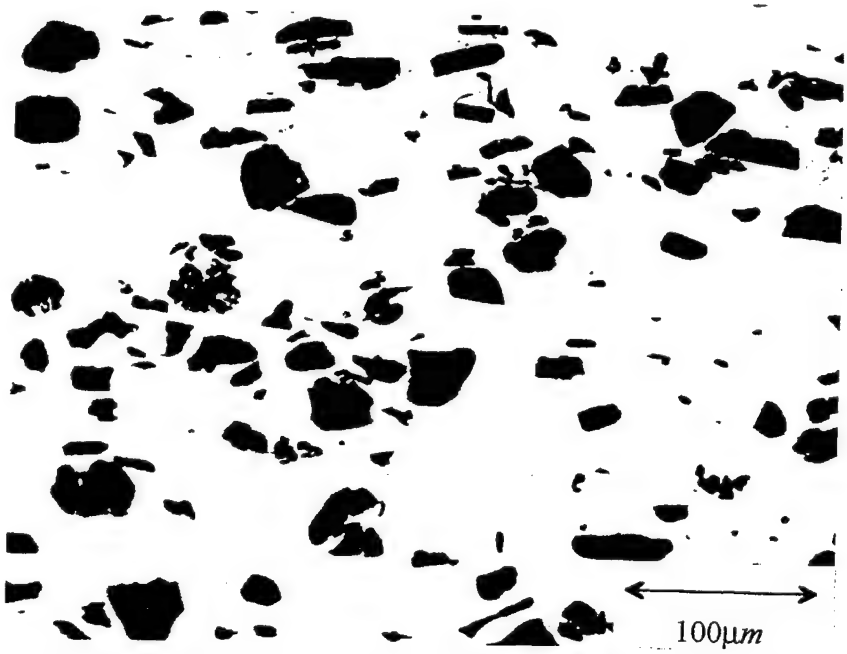

Figure 17: **Optical Micrograph of the Al 6061-20 v/o Al_2O_3 MMC Which Has Been Processed Only by Extrusions (Underaged Condition, Gage Section).**

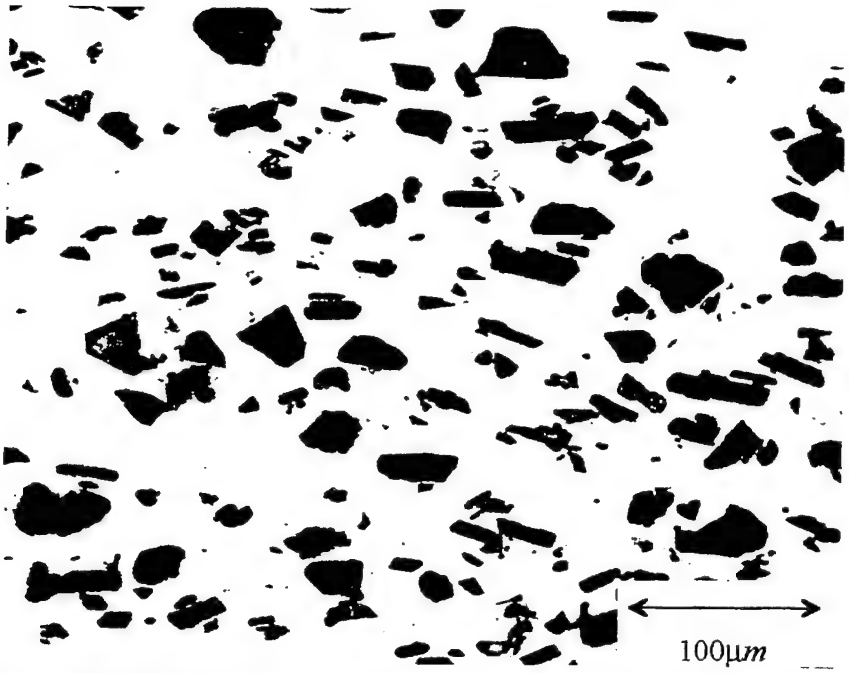

Figure 18: **Optical Micrograph of the Al 6061-20 v/o Al_2O_3 MMC Which Has Been Processed by Extrusions and Draw/Anneal Cycles (Underaged Condition, Gage Section).**

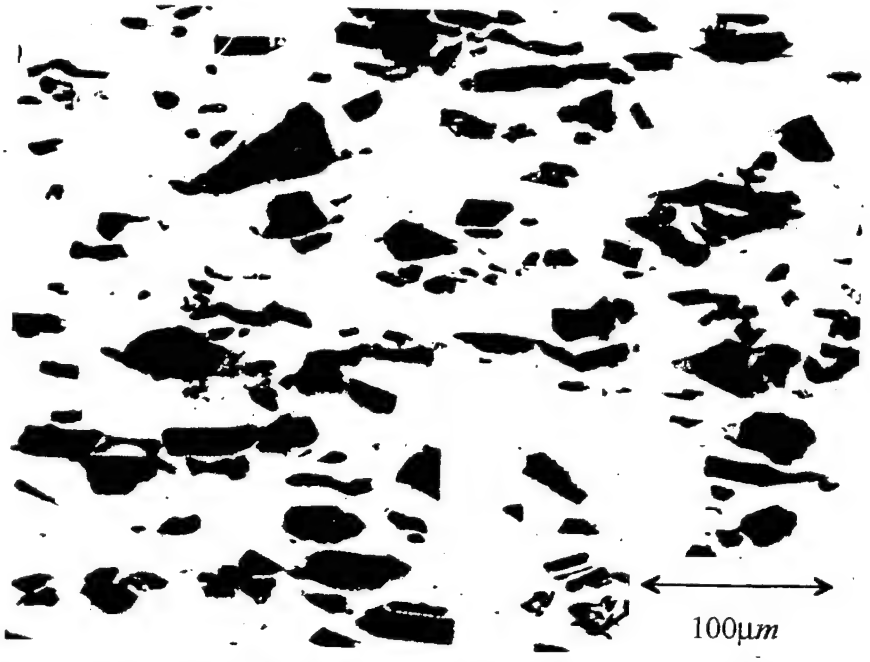

Figure 19: **Optical Micrograph of the Al 6061-20 v/o Al_2O_3 MMC Which Has Been Processed by Extrusions and Draw/Anneal Cycles (Peak Aged Condition, Gage Section).**

perpendicular to the tensile axis. The absence of cracked particles before tensile testing and the orientation of the cracks in the deformed gage sections lead to the conclusion that the cracks resulted from the effective transfer of load during tensile testing. In the Al 6061-10 v/o Al_2O_3 MMC which has undergone cold drawing and annealing operations, the banding of particles is evident as it was in the buttonhead ends (Figures 14 and 15). Also evident in these micrographs is void formation within clusters of particles. For all other samples, the only voids observed are those found between the fragments of cracked particles. Polarized light micrographs of all samples (Figures 20-27) show the grain structure of each gage section. The grains in the underaged materials are slightly more elongated, indicative of the greater ductility at this stage of aging. The existence of a large number of cracked particles in all gage sections examined here suggests a closer examination of the possible effects of these defects. Of primary concern is the possibility of fracture in the matrix due to unstable crack growth. If the crack in a particle is considered to be an embedded matrix crack, the stress intensity K associated with such a defect may be estimated by:

$$K = \sigma\sqrt{\pi a} \qquad (3.1)$$

where is the applied stress and a is half the length of the crack. Substituting 10 μm for crack length (the maximum crack size for the Al 6061-20 v/o Al_2O_3 MMC is 2a=20 μm , the particle diameter) and the nominal ultimate tensile strength of 6061 aluminum (380 MPa) for the stress σ , a K value of 2.13 MPa $m^{1/2}$ results. This estimate ignores stress concentrations associated with the presence of the remaining particle fragments (which certainly no longer support as great a stress after cracking). This value is well below

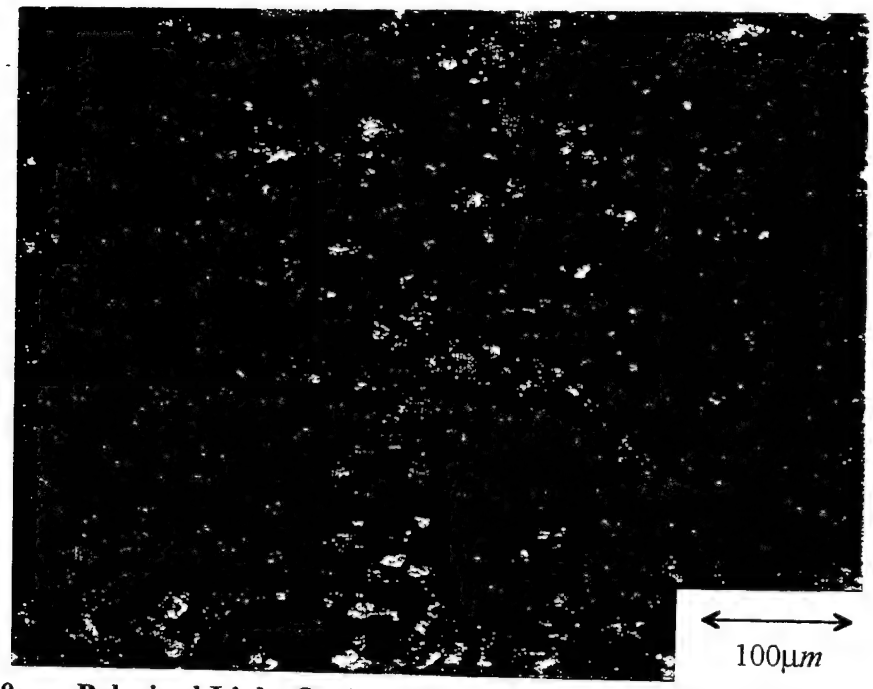

Figure 20: **Polarized Light Optical Micrograph of the Al 6061-10 v/o Al_2O_3 MMC Which Has Been Processed Only by Extrusions (Underaged Condition, Gage Section).**

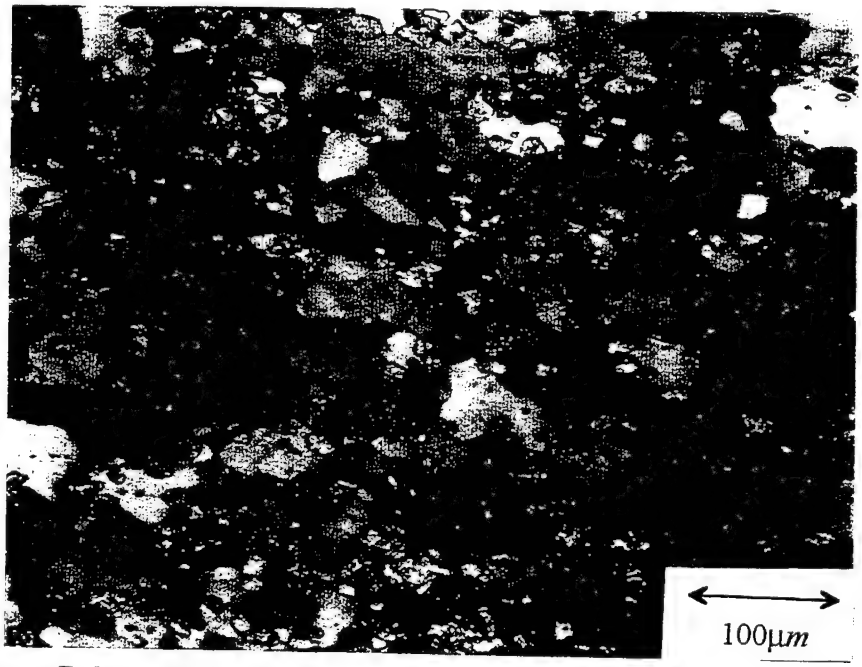

Figure 21: **Polarized Light Optical Micrograph of the Al 6061-10 v/o Al_2O_3 MMC Which Has Been Processed Only by Extrusions (Peak Aged Condition, Gage Section).**

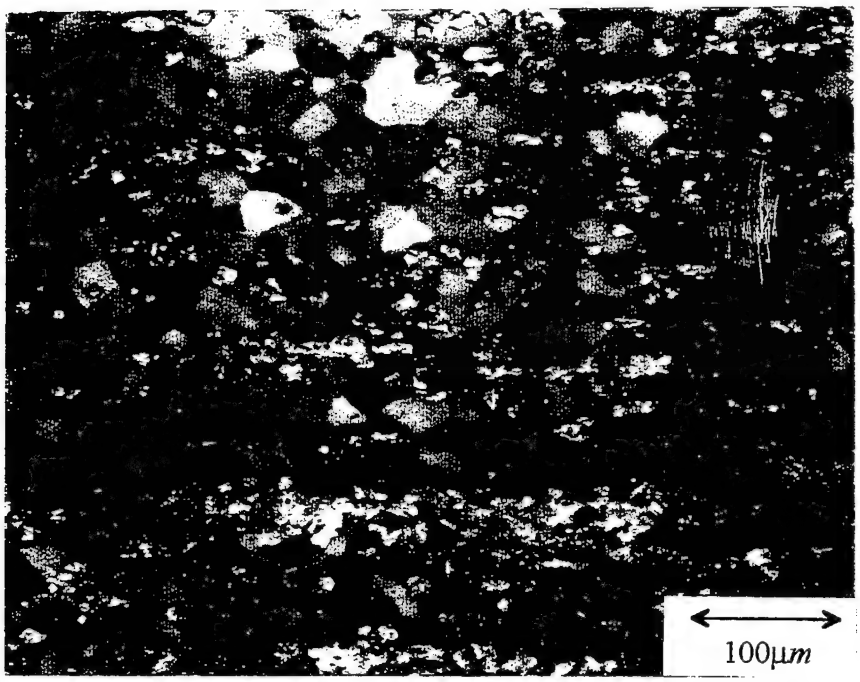

Figure 22: **Polarized Light Optical Micrograph of the Al 6061-10 v/o Al_2O_3 MMC Which Has Been Processed by Extrusions and Draw/Anneal Cycles (Underaged Condition, Gage Section).**

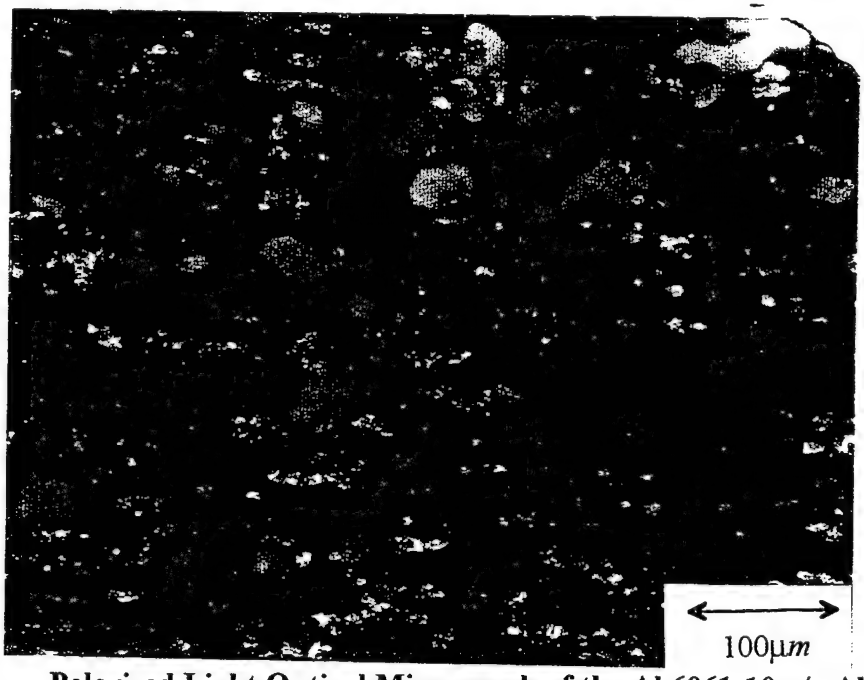

Figure 23: **Polarized Light Optical Micrograph of the Al 6061-10 v/o Al_2O_3 MMC Which Has Been Processed by Extrusions and Draw/Anneal Cycles (Peak Aged Condition, Gage Section).**

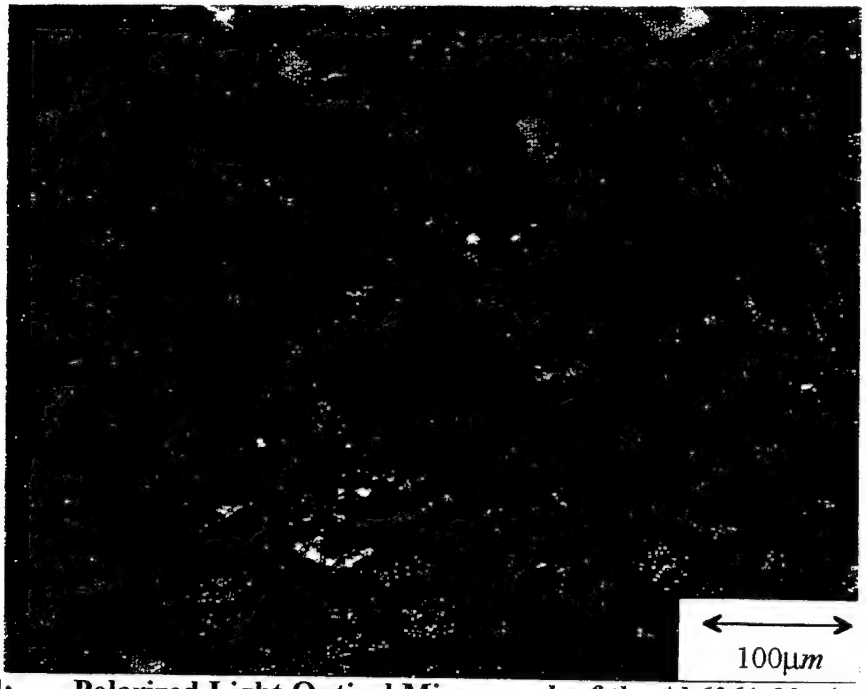

Figure 24: **Polarized Light Optical Micrograph of the Al 6061-20 v/o Al_2O_3 MMC Which Has Been Processed Only by Extrusions (Underaged Condition, Gage Section).**

Figure 25: **Polarized Light Optical Micrograph of the Al 6061-20 v/o Al_2O_3 MMC Which Has Been Processed Only By Extrusions (Peak Aged Condition, Gage Section).**

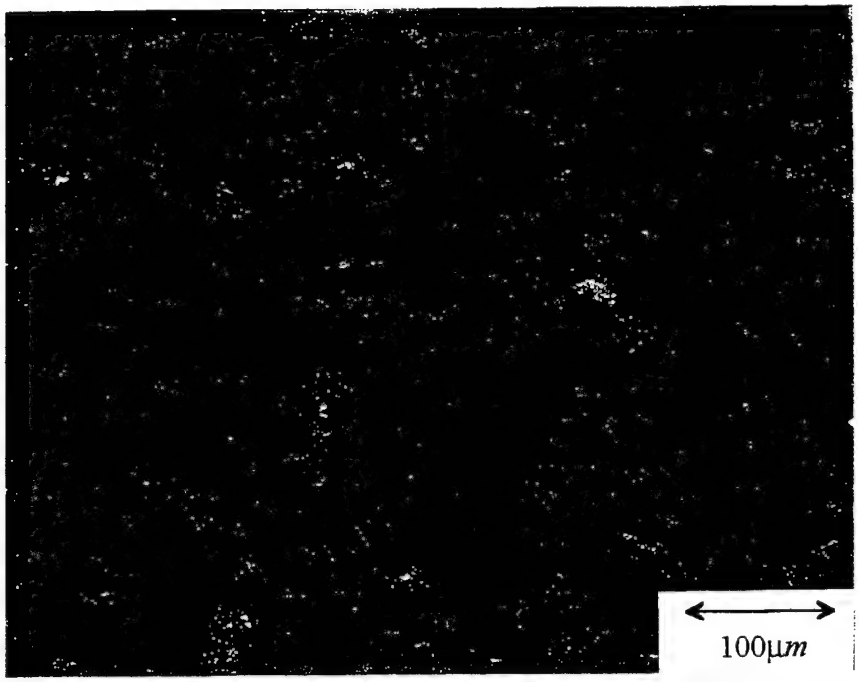

Figure 26: **Polarized Light Optical Micrograph of the Al 6061-20 v/o Al_2O_3 MMC Which Has Been Processed by Extrusions and Draw/Anneal Cycles (Underaged Condition, Gage Section).**

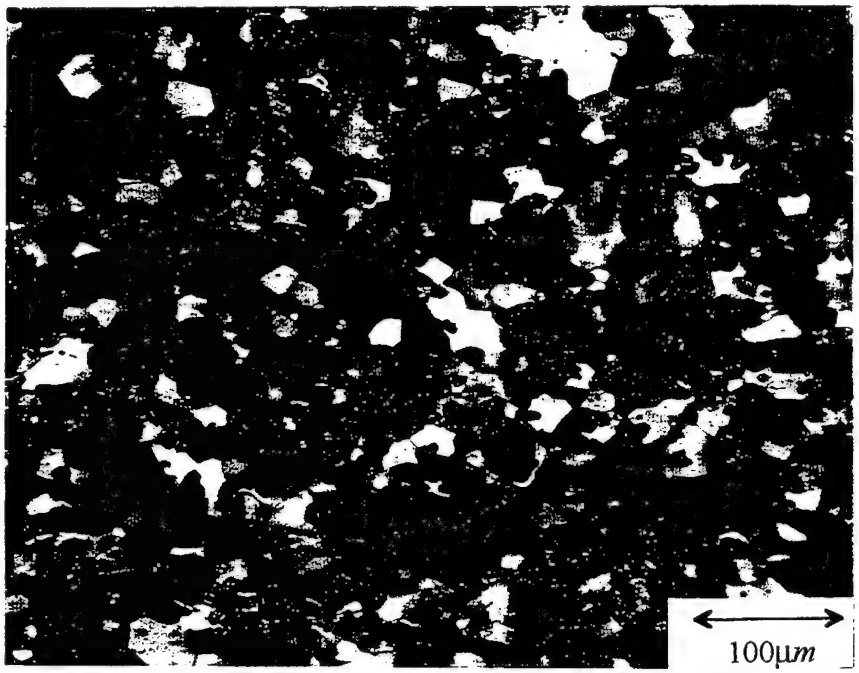

Figure 27: **Polarized Light Optical Micrograph of the Al 6061-20 v/o Al_2O_3 MMC Which Has Been Processed by Extrusions and Draw/Anneal Cycles (Peak Aged Condition, Gage Section).**

expected K_{IC} values for peak-aged 6061 aluminum, so unstable crack growth is not expected. In fact, careful examination of microscopy in the gage sections reveals blunting of cracks by plastic flow in the matrix.

SEM fractography was carried out on all samples. In all cases, dimpled features indicative of ductile fracture in the matrix were observed. At the bottom of many of these dimples were fractured Al_2O_3 particles. This suggests that the fractured particles acted as void nucleation sites. Figures 28 and 29 are typical of all fracture surfaces. The SEM fractography combined with the optical microscopy indicate that failure occurred in the following sequence as shown schematically in Figure 30. First, load is effectively transferred to the reinforcement particles. As the matrix begins deforming plastically, matrix flow occurs to accommodate the nondeforming particles. Particle cracking occurs throughout the gage section as a result of effective load transfer. As the fragments of cracked particles are pulled apart, voids are formed. When a sufficient number of particles along the plane of fracture are cracked, microscopic necking of the ligaments between cracked particles occurs. Finally, the MMC fails by ductile tearing of the matrix resulting in linkage of the voids between cracked particle fragments.

Observations of optical microscopy at various distances from the fracture surfaces indicated that the spacing between the fragments of cracked particles was a maximum near the fracture surface and decreased with increasing distance from the fracture surface (Figures 31 and 32). This suggests a possible correlation between spacing of particle

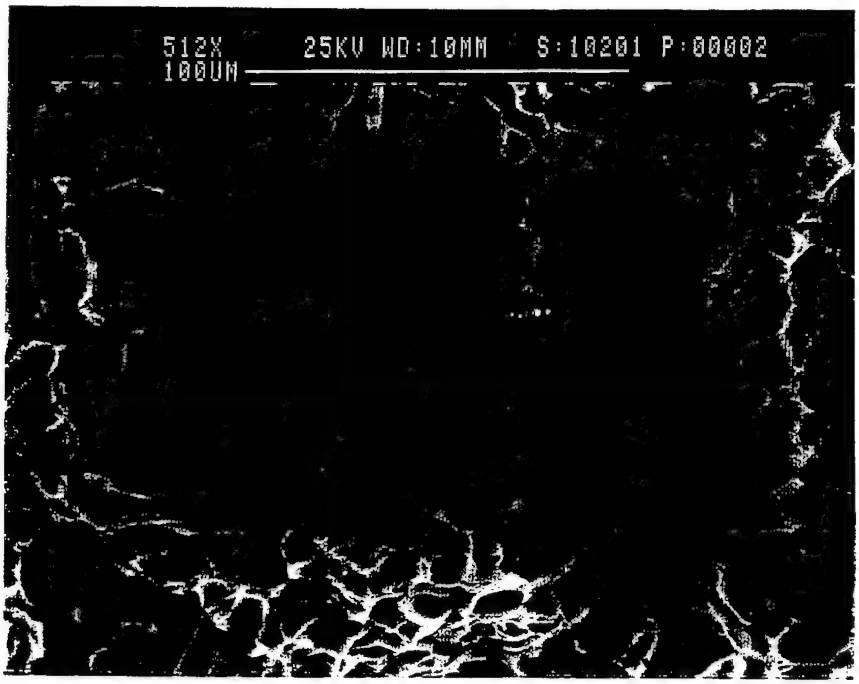

Figure 28: **SEM Micrograph of the Fracture Surface of the Al 6061-10 v/o Al_2O_3 MMC That Has Been Processed by Extrusions and Draw/Anneal Cycles (Underaged Condition).**

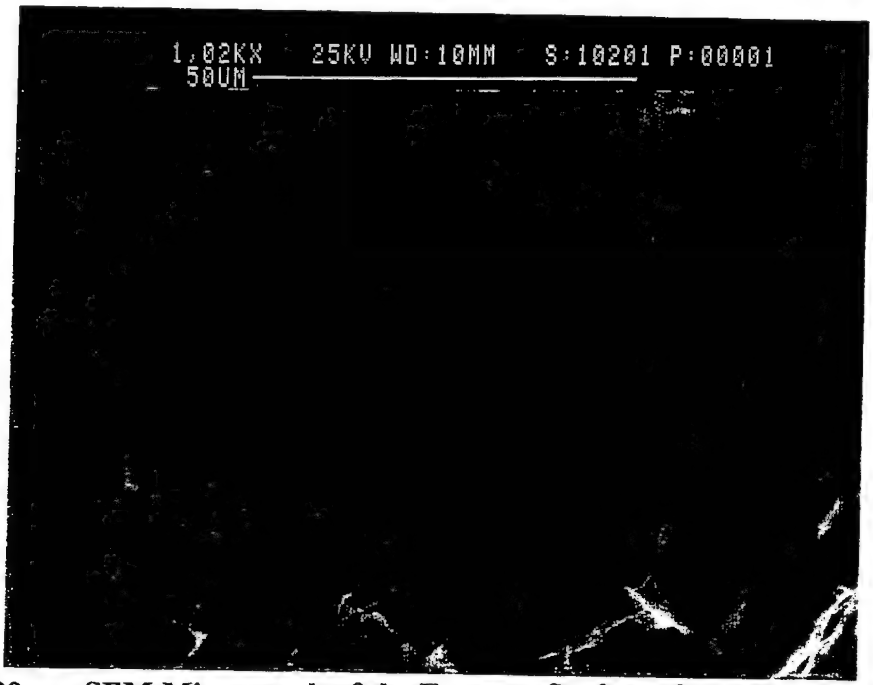

Figure 29: **SEM Micrograph of the Fracture Surface of the Al 6061-10 v/o Al_2O_3 MMC That Has Been Processed by Extrusions and Draw/Anneal Cycles (Underaged Condition).**

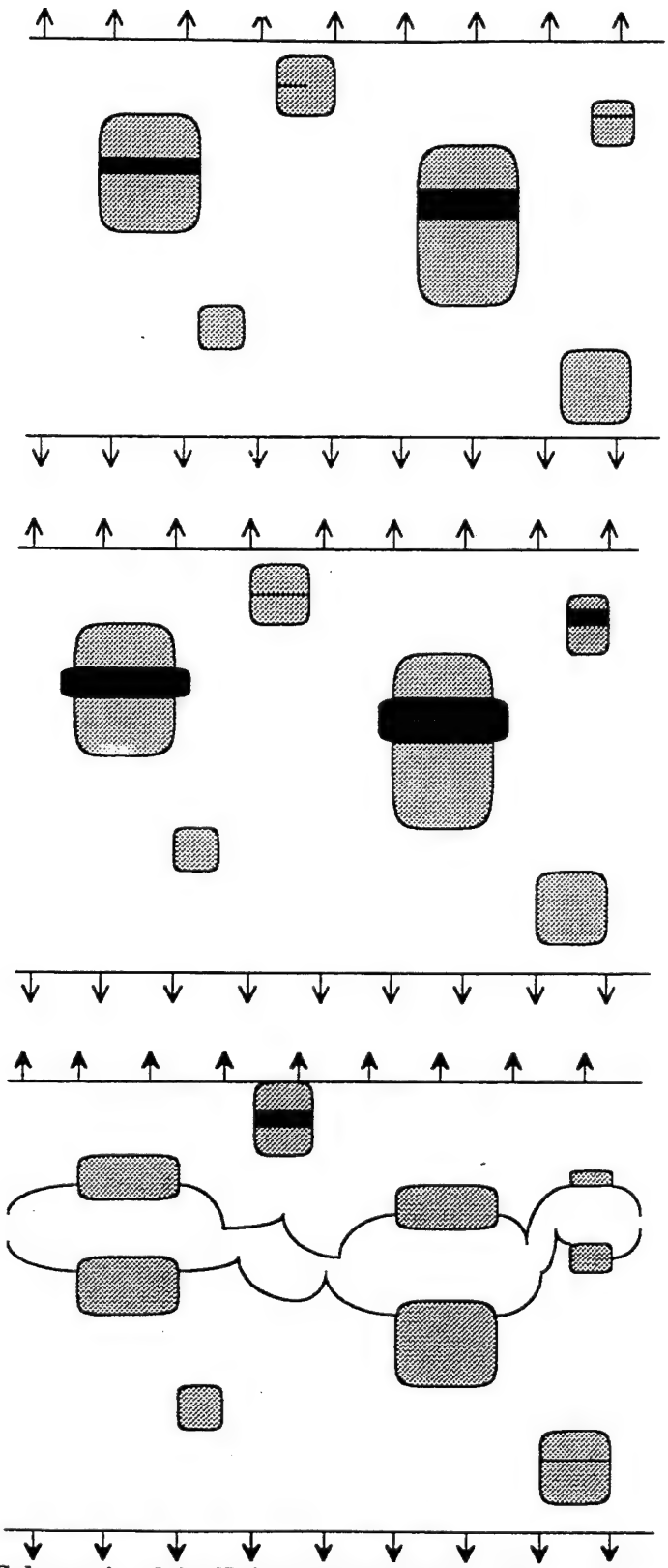

Figure 30: **Schematic of the Failure Mechanism in These Metal Matrix Composites.**

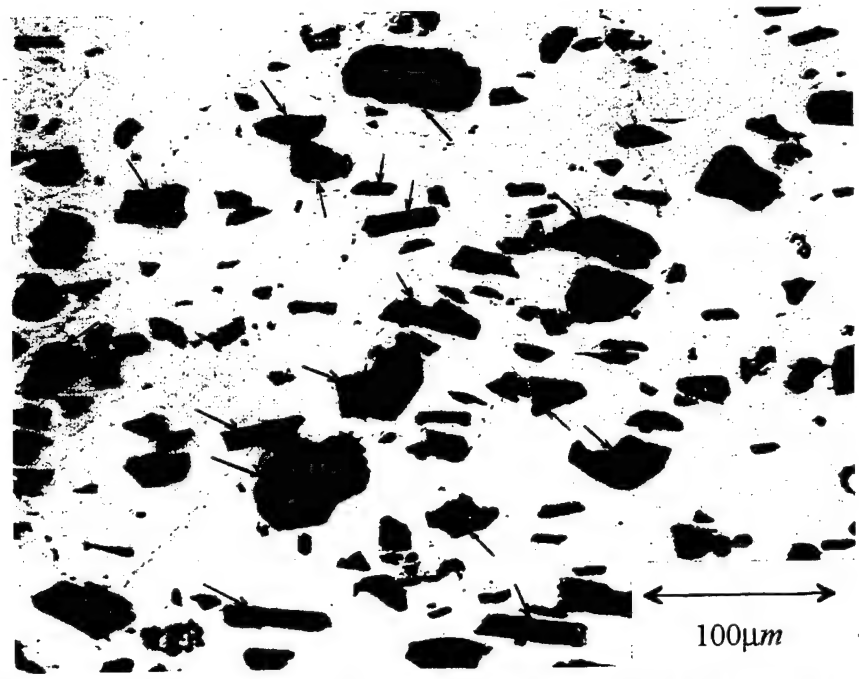

Figure 31: **Optical Micrograph of the Al 6061-20 v/o Al_2O_3 MMC That Has Been Processed Only by Extrusions, Near the Fracture Surface (Peak Aged Condition). Arrows Denote Cracked Particles.**

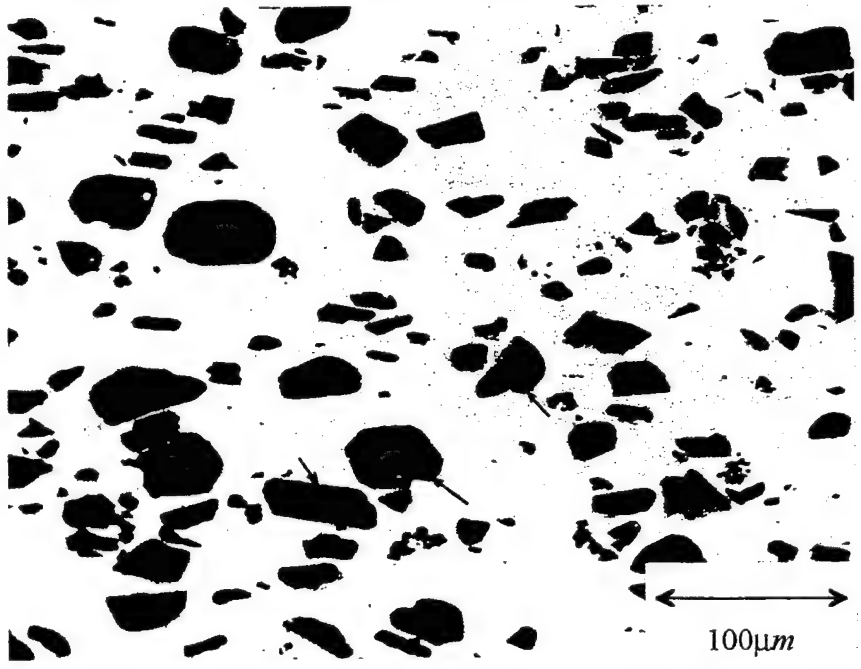

Figure 32: **Optical Micrograph of the Al 6061-20 v/o Al_2O_3 MMC That Has Been Processed Only by Extrusions, Far From the Fracture Surface (Peak Aged Condition). Arrows Denote Cracked Particles.**

fragments and local strain. Local strain measurements were obtained as indicated below. The associated true strain was calculated by the equation:

$$\varepsilon = \ln(1 + (\Delta L/L_0)) \qquad (3.2)$$

where Δ L is the spacing between particle fragments and L_0 is the length of the particle in the tensile direction before tension (the difference between the measured final length and Δ L). Average values of local strain were determined from two or three micrographs for each specimen. The reduction in area (RA) for each specimen was also calculated using the equation:

$$RA = \ln(A_f/A_o) = 2\ln(D_f/D_o) \qquad (3.3)$$

where D_f is the diameter of the sample after tensile failure and D_0 is the diameter of the sample before tension testing. The resulting measurements for Al 6061-10 v/o Al_2O_3 MMCs are summarized in Figure 33 and those for Al 6061-20 v/o Al_2O_3 MMCs in Figure 34. Elongation and reduction in area were also calculated for all materials and appear in Figures 33 and 34. In all cases, the elongation and local strain measurement away from the fracture surface are higher for peak aged materials than for materials which have been subjected to the same TMP but underaged. This reflects the loss of ductility in the matrix associated with aging to peak strength. The reduction in area data is on the order of the elongation data for each sample. In ductile tensile failure in unreinforced materials, reduction in area figures are normally much higher than elongation figures. This is due to the observed necking resulting from unstable plastic deformation in unreinforced materials. In these materials, however, very little external macroscopic necking is observed. Instead, unstable plastic deformation occurs by internal necking. This internal necking results in

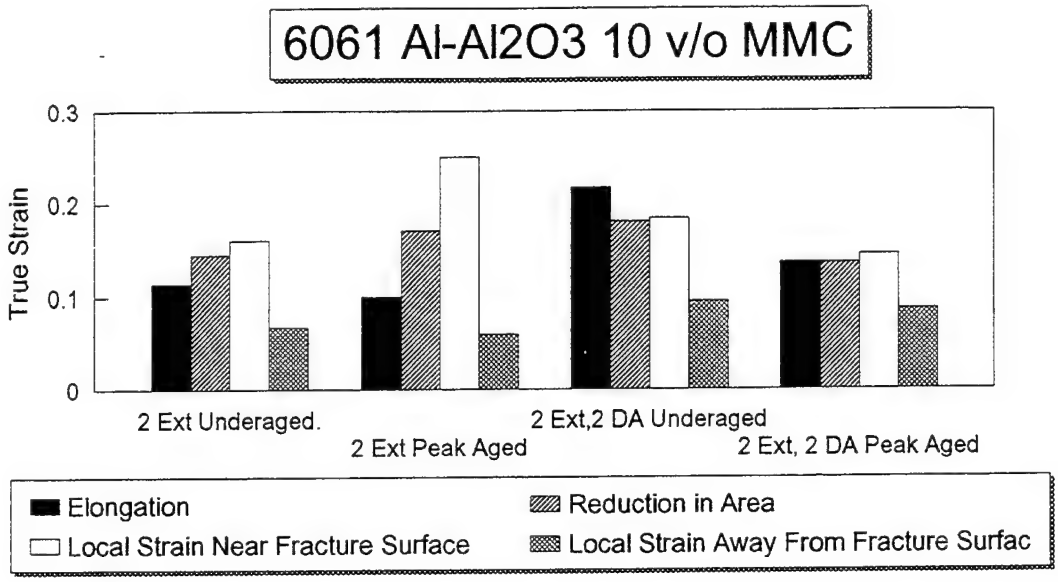

Figure 33: Strain Measurements for the Al 6061-10 v/o Al_2O_3 MMC.

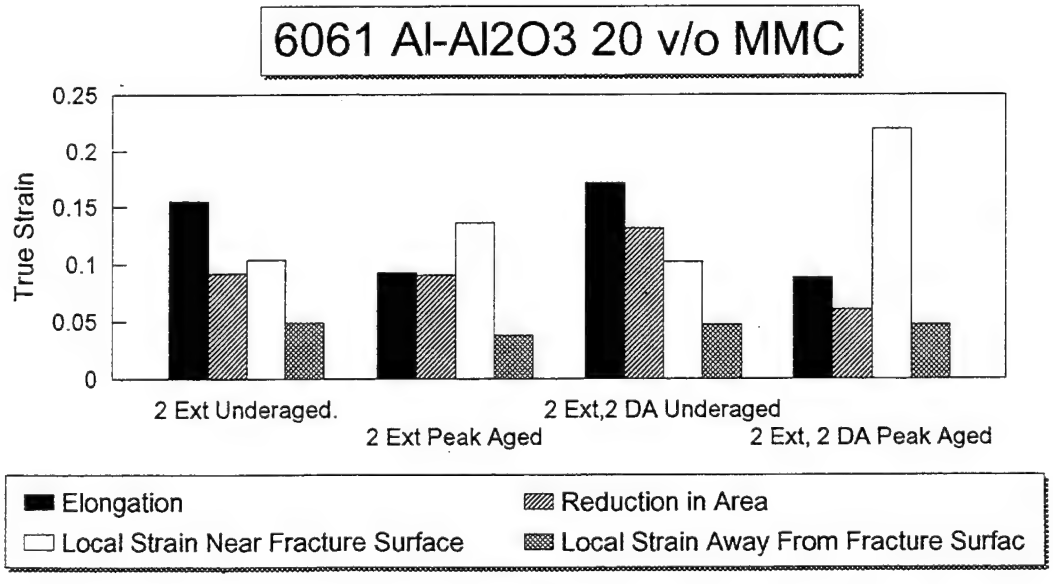

Figure 34: Strain Measurements for the Al 6061-20 v/o Al_2O_3 MMC.

much higher local strain measurements near the fracture surface than away from the fracture surface. In all cases except the 6061-10 v/o Al_2O_3 MMC which has experienced cold drawing and annealing operations, the local strain measurements near the fracture surface are higher in the peak aged condition. Because the matrix in these materials is stronger and less ductile, particle cracking begins at a lower strain than in the underaged materials. Particle fragments are therefore pulled apart during a relatively greater proportion of the tension test, resulting in greater local strain measurements. In the 6061-10 v/o Al_2O_3 MMC which has seen drawing and annealing operations, local strain measurements were somewhat suspect due to the formation of large voids within particle clusters. Only particles outside of clusters were used for local strain measurements.

A concern resulting from this part of the study is the measurement of ductility in these materials. Percentage elongation, conventionally used for measurement of tensile ductility, may not be appropriate. Some of the measured elongation results from volume dilatation due to void formation throughout the deforming gage section. Even neglecting this effect, elongation following significant particle cracking may not constitute useful "ductility".

IV. REDISTRIBUTION OF REINFORCEMENT PARTICLES DURING PROCESSING

A. INTRODUCTION

In general, whether consolidated initially by powder metallurgy or melt-processing methods, reinforcing particles tend to be non-uniformly distributed in clusters in as-consolidated particle-reinforced MMCs. Although it is generally agreed that large amounts of straining are necessary to produce a uniform and homogeneous particle distribution, the mechanisms by which this redistribution occurs have not been addressed. It was the goal of this portion of the study to initiate an experimental investigation of the mechanisms by which particles are redistributed during processing. Specifically, the role of temperature in these processes was examined. This followed the observation reported in the previous chapter, namely that deformation processing via low temperature drawing resulted in a banded particle distribution while hot-extrusion produced a more uniform particle distribution.

B. EXPERIMENTAL PROCEDURE

The material used for this portion of the study was the 6061-10 v/o Al_2O_3 MMC. This material had a less homogeneous particle distribution before processing than did the 6061-20 v/o Al_2O_3 MMC and seemed the most promising for observing particle redistribution mechanisms.

Several factors influenced the design of the experimental apparatus for this portion of the study. First, in order to investigate mechanisms at work, the microstructures of specimens needed to be recorded at many successive stages of processing. It was desired to observe the same sample at various stages of processing to avoid errors caused by differences among seperate samples. Tracking specific groups of particles at various stages of processing was also a goal. Even if this were not possible, it was desired to observe the same surface at varying degrees of strain. Finally, for this study and future work, it was desired to have close control over all processing parameters. Reports of excessive die wear during extrusion of these composites [Ref. 30] suggested that repeated testing using extrusions was not practical due to the requirement to machine replacement dies. The requirement of machining a different die for each strain was another drawback of investigating extrusion operations. Previous work by Hoyt on forging and rolling operations on this MMC had demonstrated that particles were effectively redistributed during rolling operations [Ref. 1]. A channel die assembly seemed a logical solution to this list of specifications. The channel maintains the sample in a state of plain strain similar to that found in rolling operations while allowing carefully controlled strain increments to be applied and also maintaining a flat surface for microscopy.

An Instron Model 4507 testing machine with a five-zone furnace used for work on superplasticity of aluminum alloys [Ref. 31] was used. This arrangement offered close computer control of strain rates, total strain and temperature. A channel die assembly with two pushrods was designed to ensure that the straining occurred in the center of the

five-zone furnace (Figure 35). The long pushrod assemblies, while necessary in order to use the Instron/furnace assembly, introduced the possibility of buckling failure during compression. Due to availability and adequate high temperature properties, Type 304 stainless steel pushrods were chosen. The load cell in use on the Instron testing machine was rated to 200 kN. Using this load and a factor of safety of two, the necessary pushrod radius to avoid buckling was calculated by the relationship:

$$P_{cr} = \frac{\pi^2 EI}{L_e^2} \tag{4.1}$$

where L_e is the effective length (twice the length of the rod or 0.762 m), E is the elastic modulus of Type 304 stainless steel (190 GPa), P_{cr} is the maximum load times the factor of safety (400 kN) and I is the polar moment of inertia given by:

$$I = \frac{\pi r^4}{2} \tag{4.2}$$

Combining Equations (4.1) and (4.2), an equation for required radius to prevent buckling was found:

$$r = \left(\frac{2P_{cr}L_e^2}{\pi^3 E} \right) \tag{4.3}$$

By substituting the given values, a required radius of 16.76 mm was found. Next, the necessary radius to prevent compressive failure was calculated from:

$$\sigma = \frac{P}{\pi r^2} \tag{4.4}$$

Again using a factor of safety of two, the required radius was found to be 22.13 mm. An actual radius of 22.2 mm (1.75 in diameter) was used.

The previous Euler buckling calculations assumed perfect alignment. If the sample were not placed exactly in the center of the channel die, eccentric loading could result. The lateral displacement resulting from an eccentric load is given by:

$$y_m = e[\sec(\frac{\pi}{2}\sqrt{\frac{P}{P_{cr}}}) - 1] \tag{4.5}$$

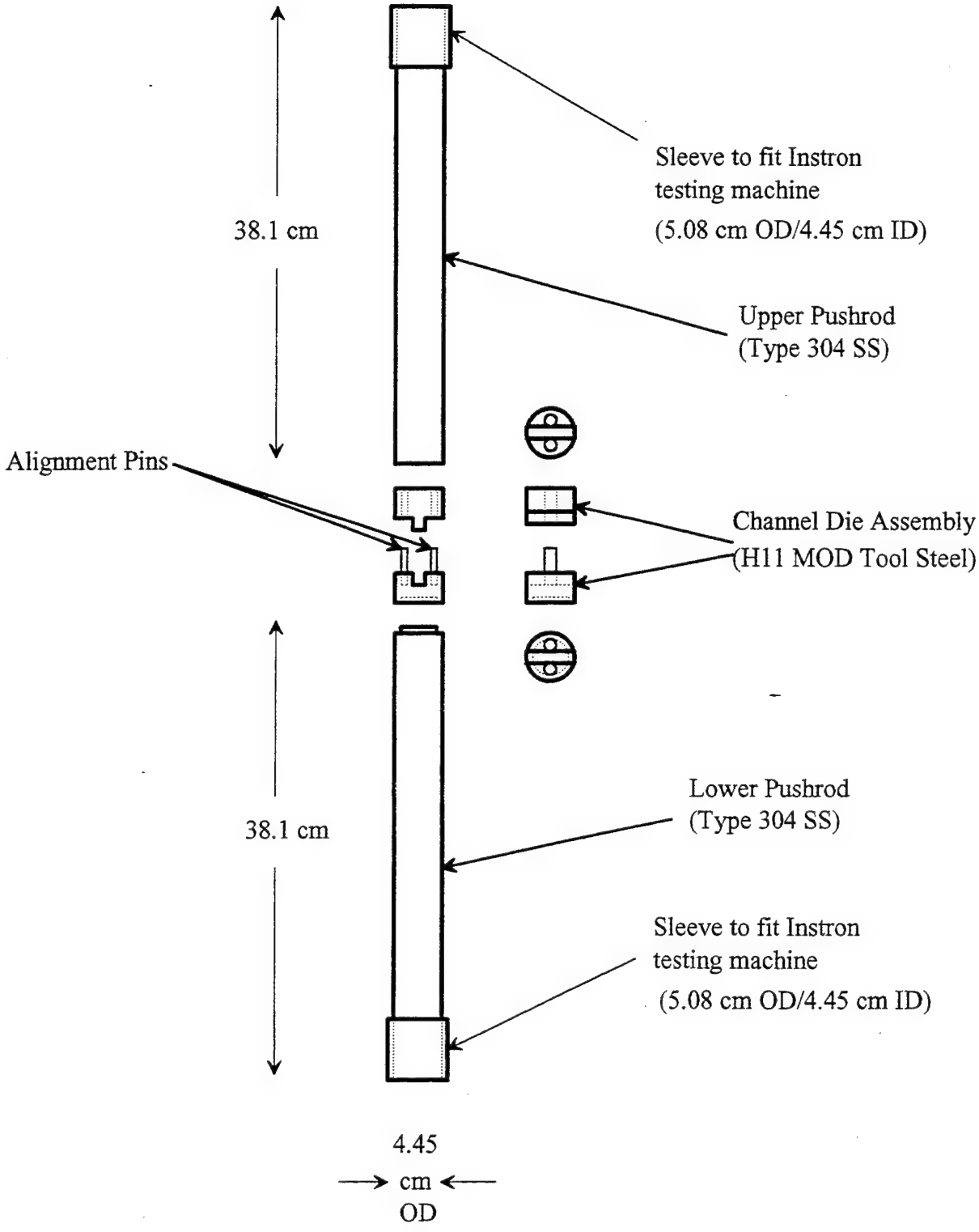

Figure 35: Channel Die/Pushrod Assembly.

where P_{cr} is given by Equation (4.1), e is the eccentricity of the load, and P is the actual load. The maximum normal stress resulting from this lateral displacement is given by:

$$\sigma_m = \frac{P}{A}[1 + \frac{e}{r}\sec(\frac{\pi}{2}\sqrt{\frac{P}{P_{cr}}})] \quad (4.6)$$

Assuming a placement of the sample 0.5 cm from the compression axis and a load of 200 kN, a stress of σ =165MPa was calculated. This represents a factor of safety of 1.6. To achieve a factor of safety of 2 with the same eccentricity, the maximum load is approximately 150 kN. This limit was adopted for all compression tests using this apparatus. For this load and eccentricity, the lateral displacement from Equation (4.5) is 0.85 mm. This represents a 0.2 % deflection, which was considered satisfactory.

Although the use of a channel die instead of extrusions significantly reduced the die wear problem, it was still desired to avoid wear and the time consuming process of machining new channel dies. Although it was reported by Jeffrey and Holcomb that cermets were preferred for maximum die life [Ref. 30], it was decided that a tool steel would suffice for this work. The major factors affecting this decision were availability and machinability. An H-11 modified tool steel was chosen for the die. After machining in accordance with Figure 35, the die was given a hardening heat treatment, followed by air cooling in still air and double tempering [Ref. 29]. Hardening and annealing heat treatments were conducted in a Vulcan NEY furnace. To minimize oxidation, nitrogen was bled into the furnace during all heat treating.

During sample compression, the sample was placed into the channel in the lower half of the die following lubrication. The upper portion of the die was then placed tongue side down onto the sample. The die assembly was next placed onto the lower pushrod.

The entire assembly was preloaded in compression on the Instron testing machine. If elevated temperature testing were to be conducted the five-zone furnace could be closed around the assembly and brought up to temperature. Once at temperature, the sample was compressed until the desired strain was acheived.

For compression temperatures up to 200°C, Teflon tape was used for lubrication. When Teflon tape was wrapped around samples before processing, the samples could be removed either by hand or with a small press. Graphite was less effective as a lubricant. Although Teflon tape was sufficient for this study, higher temperature compression will require MoS_2 as a lubricant.

An experiment was designed to allow observation of particle distribution and matrix microstructure at various stages of processing. The details of the experiment are presented in flowchart form in Figure 36. Conventional optical and polarized light microscopy was obtained at each stage using procedures delineated in Chapter III. Because the same samples were to be strained several times, they were not cold mounted. Anodizing was performed on each sample by making electrical contact with a metal C-clamp. Care was taken to avoid contact between this C-clamp and the electrolyte.

Billets, 76 mm x 51 mm x 44 mm in size, of Al 6061-10 v/o Al_2O_3 MMC were sectioned from a 838 mm x 178 mm x 51 mm section of a rolling slab by the manufacturer (DURALCAN-USA, San Diego, CA). The billets were solution heat treated for 20 hours at 530°C in a Blue-M oven, Model OV-490A-3; after solutionizing, they were transferred directly to a heated platen press. The billets were forged from an initial height of 76 mm to the height required for the strains corresponding to those in Figure 40. Hot-forging

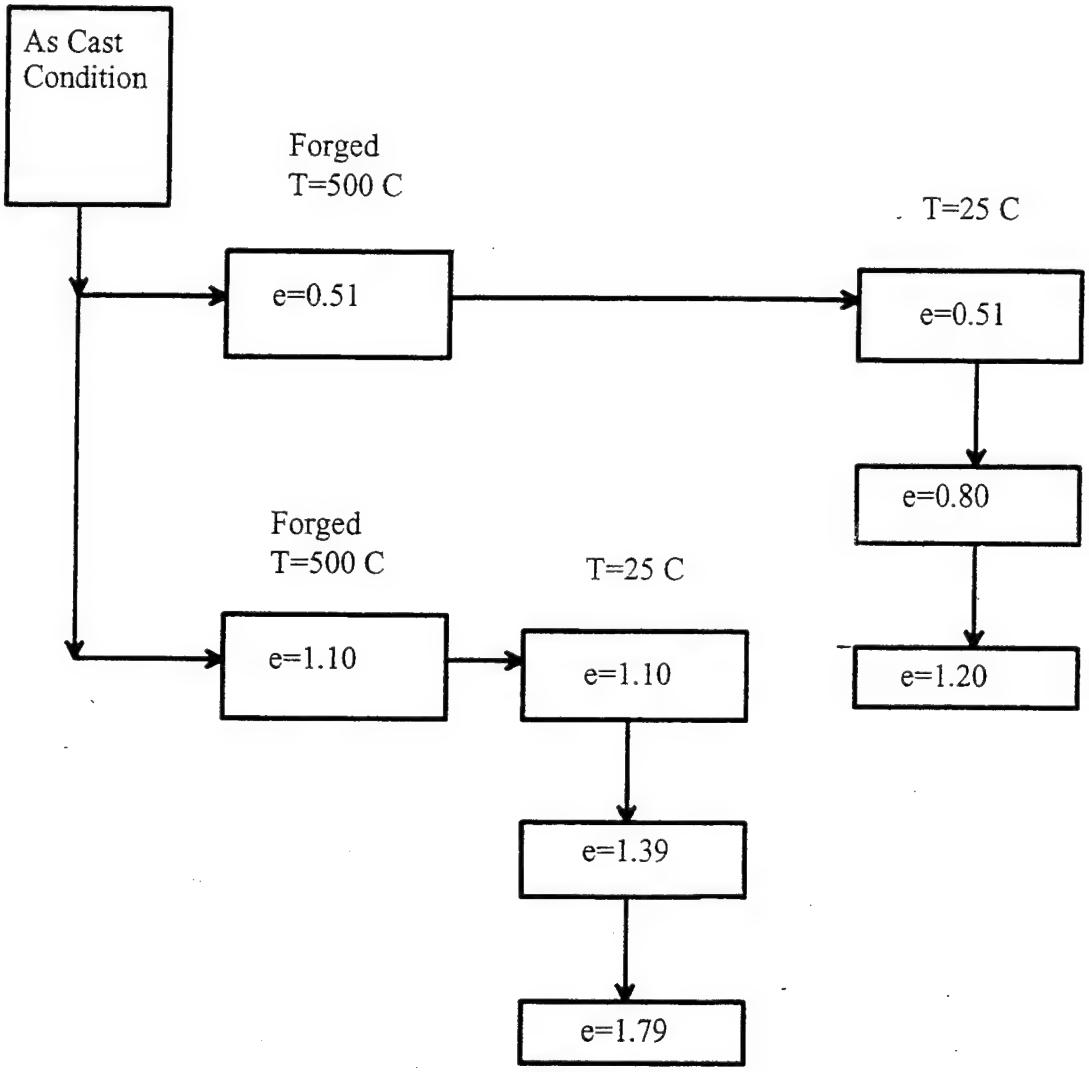

Figure 36: Flowchart of TMP Schedule for Observation of Particle Redistribution and Matrix Grain Refinement.

was carried out in accordance with the procedures developed by Hoyt [Ref. 1]. The forged billets were returned to the 530°C Blue-M oven for approximately 20 minutes and then quenched in 25°C water.

Samples were cut from the forgings to fit the channel die using an Isomet 2000 precision saw. The nominal dimensions of the samples were 23 mm x 10.5 mm x 7.6 mm. All sides of each sample were ground on a Knuth Rotor Grinder following procedures described in Chapter III. One 10.5 mm x 23 mm side was polished and anodized following each compression increment on each sample as described previously.

C. RESULTS/DISCUSSION

Polarized light microscopy of the as-cast billet (Figure 37) illustrates the large grain size and nonhomogeneous particle distribution typical of these materials before deformation processing. After hot-forging to a true strain of 0.51 (Figure 38), some refinement of the matrix grain structure due to recrystallization was noted. Also, the particle distribution is improved, but is still nonhomogeneous. Subsequent straining at room temperature in the channel die (Figures 39 and 40) results in pancaking of the matrix grains. Grains are not only flattened, but also appear to deform around clusters of particles. Slip bands are evident in the matrix. Even when deformed onward to a true strain of 1.2 (Figure 40), there is little improvement in particle distribution; clusters appear to remain undeformed during low-temperature straining while the matrix flows around these groups of particles.

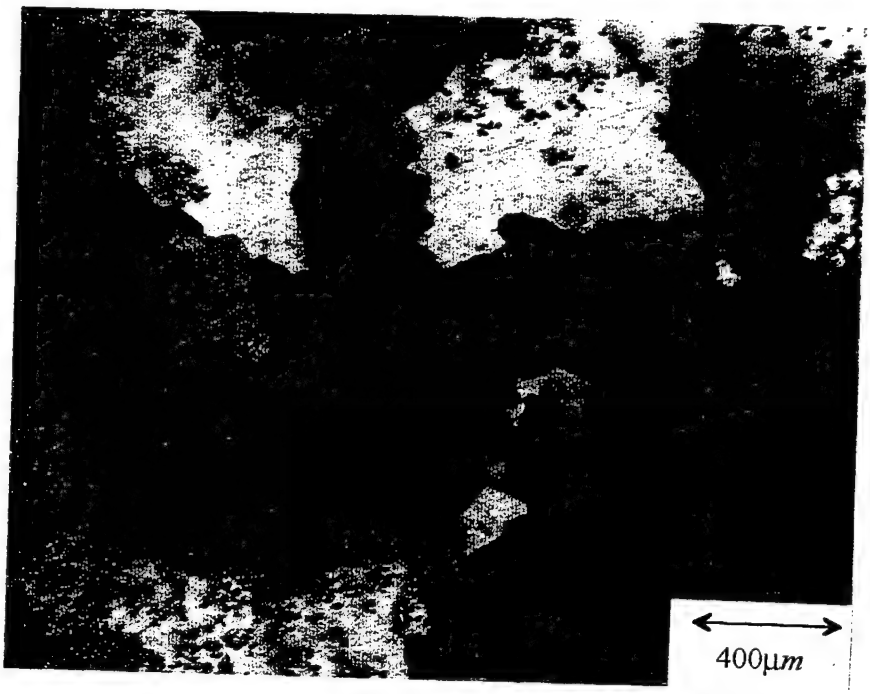

Figure 37: **Polarized Light Optical Micrograph of the as Cast Billet of Al 6061-10 v/o Al_2O_3.**

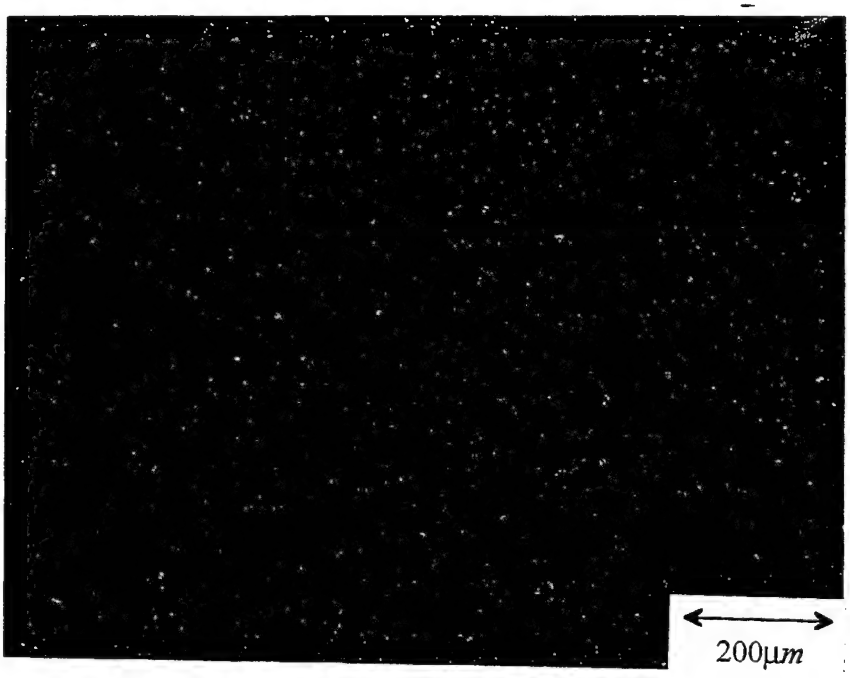

Figure 38: **Polarized Light Optical Micrograph of the Al 6061-10 v/o Al_2O_3 MMC After Hot Forging to a True Strain of 0.51.**

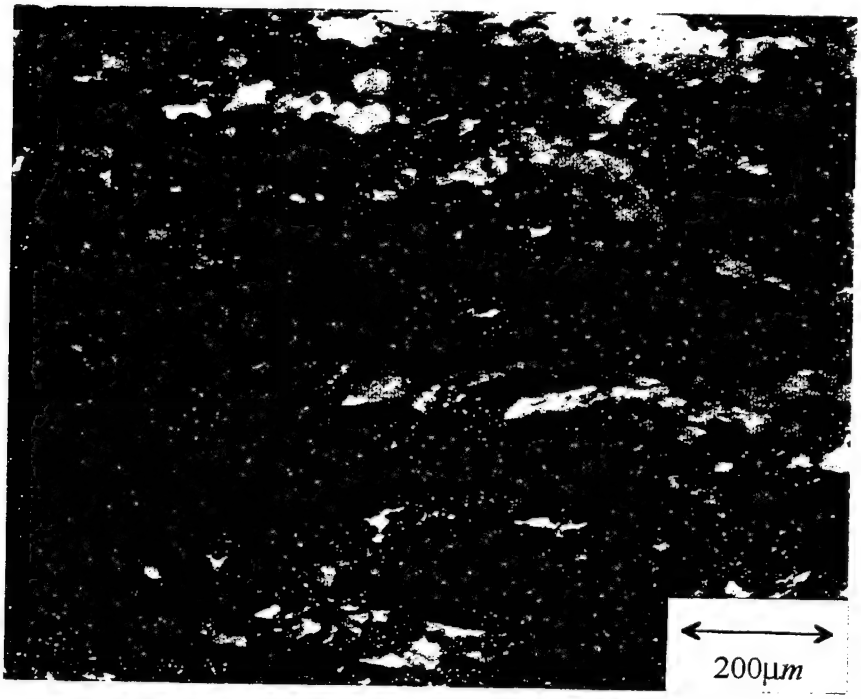

Figure 39: **Polarized Light Optical Micrograph of the Al 6061-10 v/o Al_2O_3 MMC After Hot Forging to a True Strain of 0.51 and Cold Working to a True Strain of 0.80 in the Channel Die Assembly.**

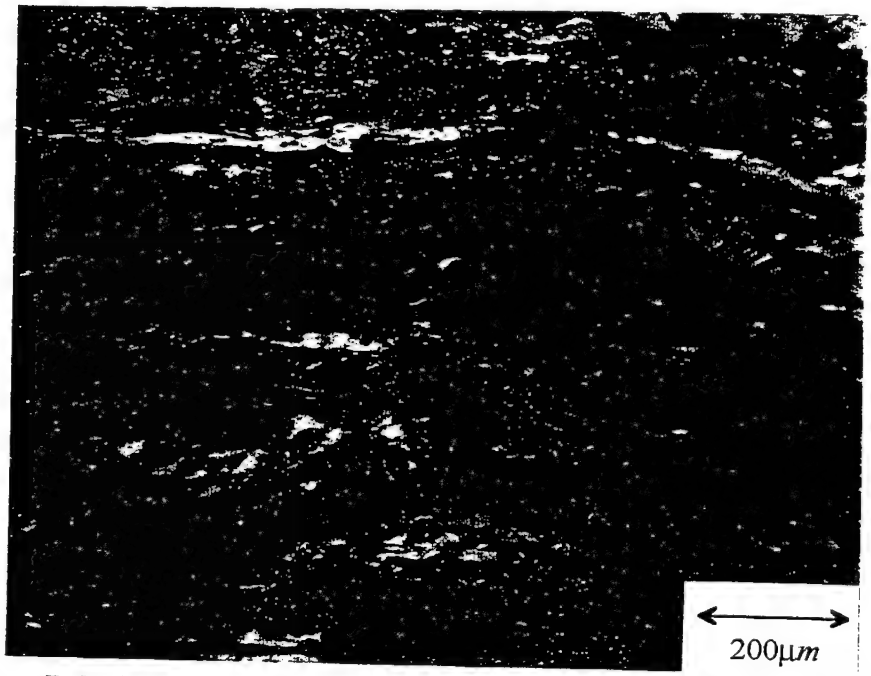

Figure 40: **Polarized Light Optical Micrograph of the Al 6061-10 v/o Al_2O_3 MMC After Hot Forging to a True Strain of 0.51 and Cold Working to a True Strain of 1.20 in the Channel Die Assembly.**

When the Al 6061-10 v/o Al_2O_3 MMC was hot-forged to a true strain of 1.1 (Figure 41), refinement of the matrix microstructure resulted. Apparently, new grains formed within particle clusters suggesting that recrystallization is occurring by Particle Stimulated Nucleation (PSN). Another possibility is increased nucleation of new grains within particle clusters due to the higher dislocation density in these clusters, leading to new nucleation sites. Further deformation of this sample at room temperature (Figures 42 and 43), however results in deformation of the matrix grains in a manner similar to that observed in cold deformation of the previous sample. Again, particle distribution is not significantly improved in the room temperature straining.

Immediately following hot forging to a strain of 1.1, the sample in Figure 41 has seen nearly the same strain as the preceding sample following completion of its hot/cold processing route (Figure 40). Higher magnification montages of these two stages (Figures 44 and 45), clearly show the benefits of hot-work on microstructural homogenization. The material that has seen only hot-forging to a strain of 1.1 (Figure 44) appears to have a more homogeneous particle distribution than the material which has reached a strain of 1.2 through a combination of hot-forging and cold deformation in the channel die (Figure 45). Additionally, the hot-forged material has a more desirable matrix microstructure in that the grain size has become more uniform as well as finer.

The observations from this portion of the study are consistent with those from the previous chapter. For the Al 6061-10 v/o Al_2O_3 MMC, hot-work leads more rapidly to a more homogeneous particle distribution. In low temperature deformation, strain

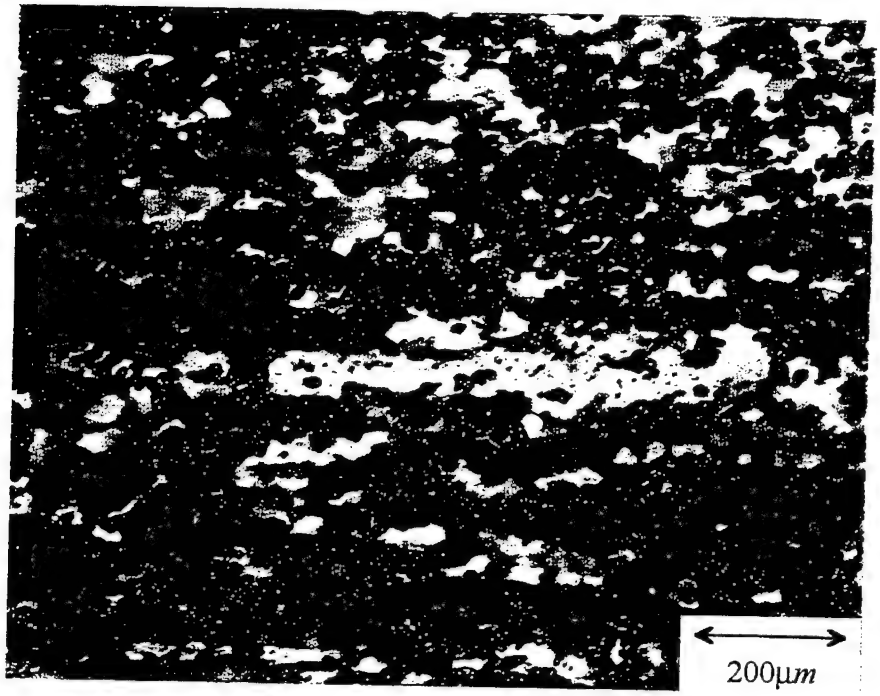

Figure 41: **Polarized Light Optical Micrograph of the Al 6061-10 v/o Al_2O_3 MMC After Hot Forging to a True Strain of 1.10.**

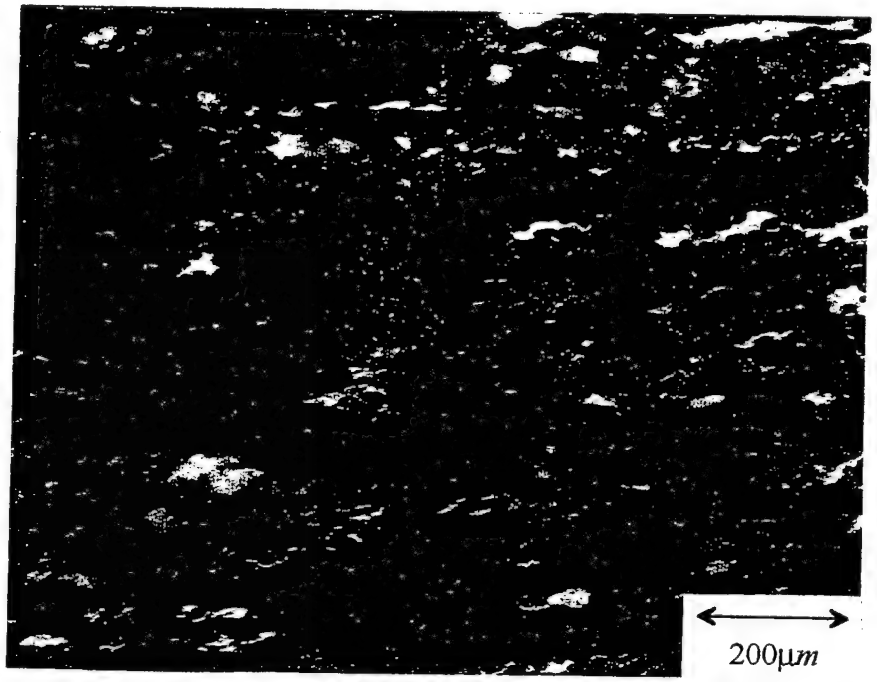

Figure 42: **Polarized Light Optical Micrograph of the Al 6061-10 v/o Al_2O_3 MMC After Hot Forging to a True Strain of 1.10 and Cold Working to a True Strain of 1.39 in the Channel Die Assembly.**

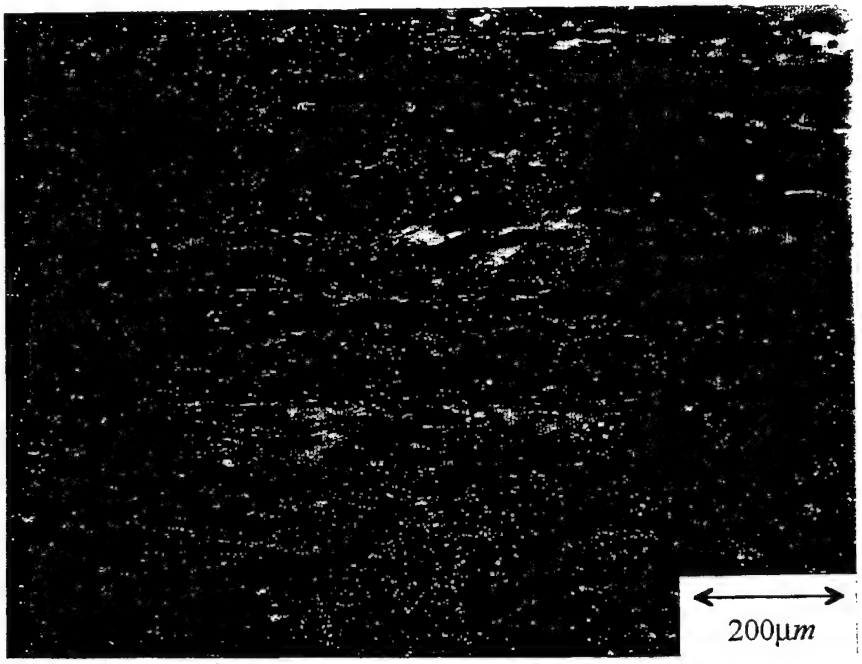

Figure 43: **Polarized Light Optical Micrograph of the Al 6061-10 v/o Al_2O_3 MMC After Hot Forging to a True Strain of 1.10 and Cold Working to a True Strain of 1.79 in the Channel Die Assembly.**

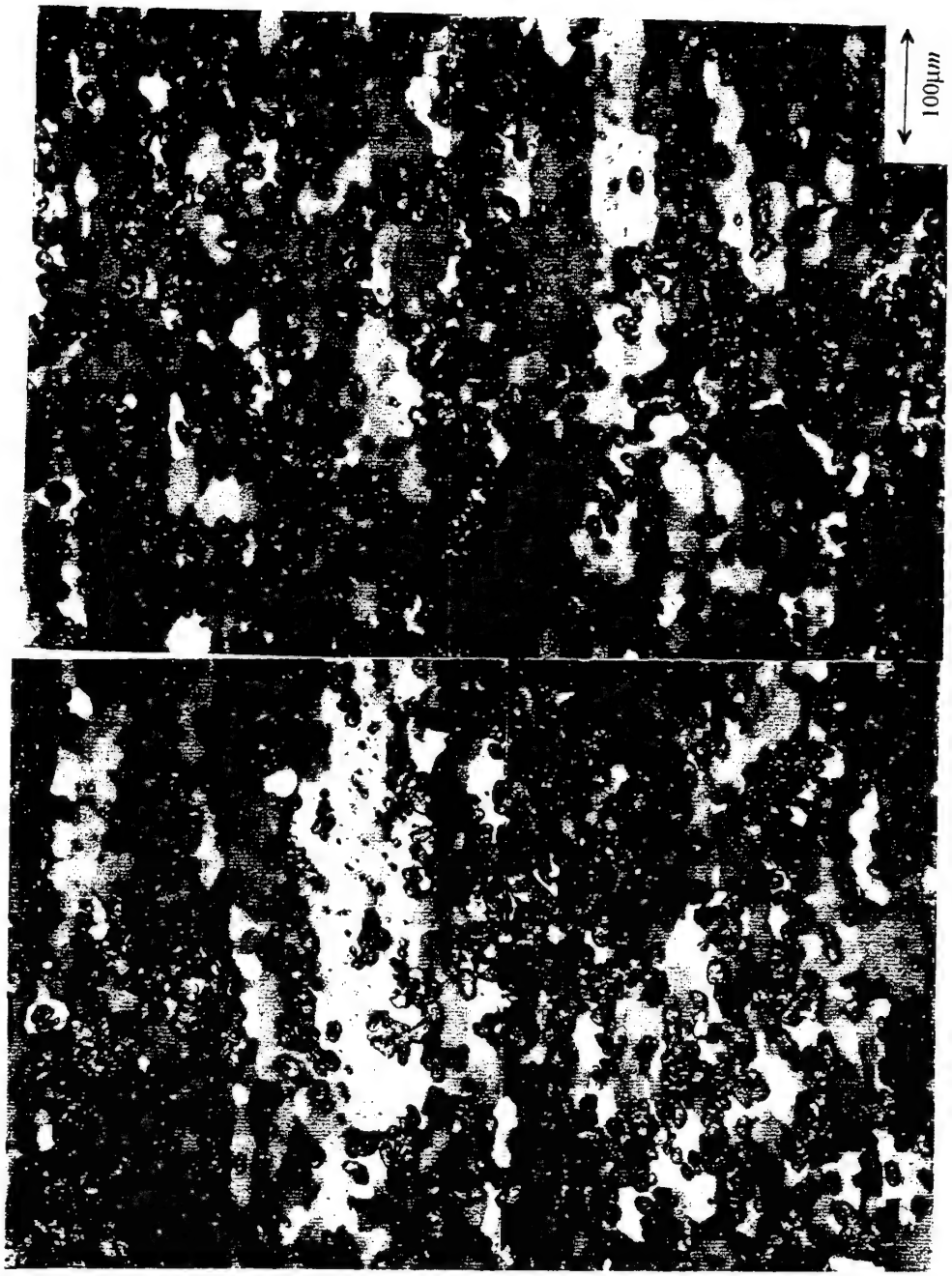

Figure 44: **Polarized Light Optical Micrograph of the Al 6061-10 v/o Al_2O_3 MMC After Hot Forging to a True Strain of 1.10.**

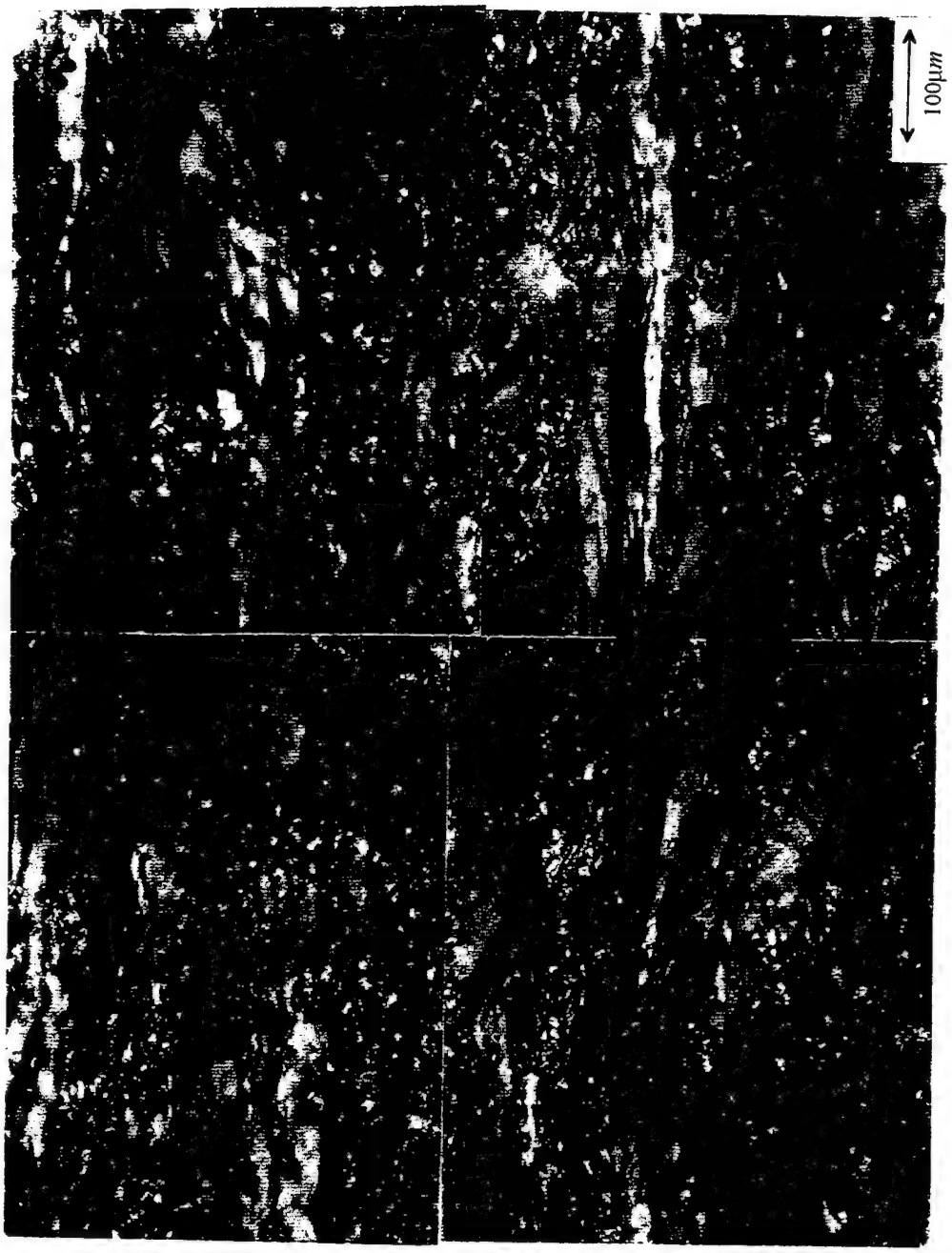

Figure 45: **Polarized Light Optical Micrograph of the Al 6061-10 v/o Al_2O_3 MMC After Hot Forging to a True Strain of 0.51 and Cold Working to a True Strain of 1.20 in the Channel Die Assembly.**

hardening occurs more rapidly within clusters of particles than in the bulk matrix. These strain hardened regions become less deformable than regions of the matrix where particles are absent. Matrix grains deform around these hardened regions during cold deformation. Plastic deformation in both regions is governed by dislocation motion. In high temperature deformation, dynamic recrystallization apparently occurs within particle clusters. Within these clusters, deformation likely occurs by a combination of grain boundary sliding and, possibly, sliding at the particle/matrix interface. Outside of particle clusters, plastic deformation occurs by dislocation motion. Grain boundary sliding exhibits a stronger dependence on stress than does dislocation deformation. Dynamic recrystallization within clusters may result in more rapid deformation within clusters than in the matrix and this, in turn, facilitates redistribution of particles. It is proposed, then, that the particles are redistributed during elevated temperature deformation processing as a consequence of the absense of strain hardening within clusters, dynamic recrystallization and the ensuing contributions of boundary and interfacial sliding mechanisms. The stress and temperature-dependence of the deformation rate for these mechanisms is certainly a factor as well.

V. SUMMARY

A. CONCLUSIONS

The following conclusions are drawn from this work:

1. Particles in these Al 6061-10 v/o Al_2O_3 and Al 6061-20 v/o Al_2O_3 MMCs are not damaged by either hot extrusions or cold drawing operations.
2. Redistribution of particles in the Al 6061-10 v/o Al_2O_3 MMC is negatively affected by the introduction of cold-drawing operations, while not influenced by cold-drawing for the Al 6061-20 v/o Al_2O_3 material.
3. Load is effectively transferred to reinforcement particles during tension testing.
4. Particles crack during tension testing, but this does not lead to unstable crack growth in the matrix of these MMCs.
5. Tensile failure in these MMCs resulted from particle cracking followed by the linkage of voids at cracked particles by ductile tearing in the matrix.
6. The fibered distribution of particles in the Al 6061-10 v/o Al_2O_3 MMC which had seen cold-drawing operations results in cavitation during tensile loading.
7. The channel die/pushrod assembly designed in this work can be used to simulate rolling operations, allowing the same sample to be observed at several stages throughout the processing routine.
8. During cold deformation, grains are flattened. Particles are not effectively redistributed.

9. During hot deformation, particles are effectively redistributed as a result of dynamic recrystallization within particle clusters, grain boundary sliding and interfacial sliding.

B. RECOMMENDATIONS

The following is a list of recommendations for further study:

1. Conduct an analysis of the local strain as measured by fractured particle spacing as a function of distance from the fracture surface for both extruded and extruded/drawn and annealed tensile samples.
2. Conduct an analysis of the percentage of cracked particles as a function of distance from the fracture surface for both extruded and extruded/drawn and annealed tensile samples.
3. Conduct incremental tensile testing on both extruded and extruded/drawn and annealed tensile samples to determine when particle cracking occurs.
4. Observe both extruded and extruded/drawn and annealed materials in a Transmission Electron Microscope (TEM) to determine any differences in precipitate morphology within the matrix.
5. Conduct a more comprehensive investigation into the effects of processing temperature on redistribution of particles and matrix microstructure using the channel die assembly.
6. Model both low temperature and high temperature deformation during processing using a Finite Element Method (FEM) analysis.

APPENDIX A:
MECHANICAL AGING RESPONSE OF THE AL 6061-10 V/O AL_2O_3 PROCESSED WITH EXTRUSIONS ONLY.

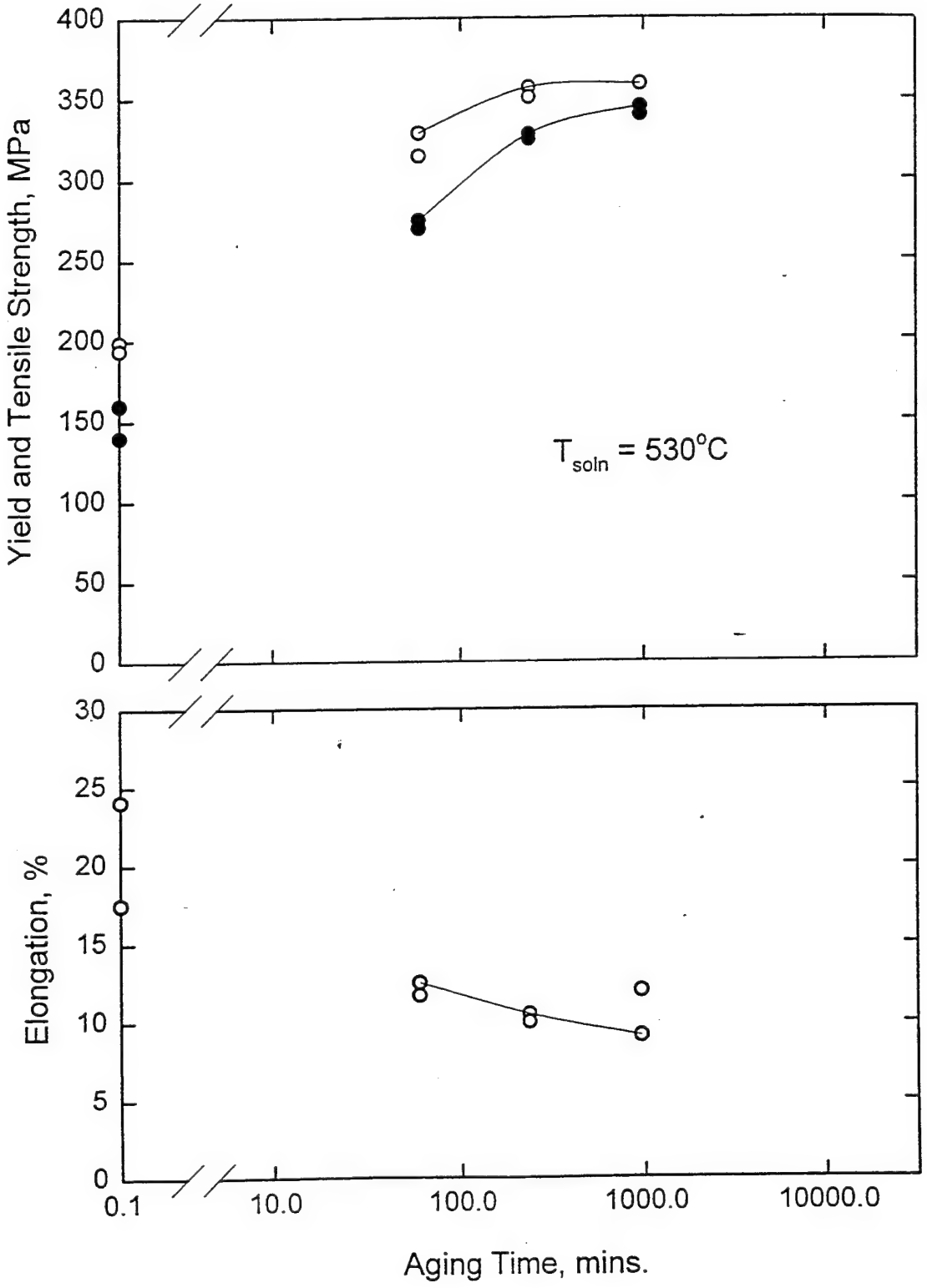

APPENDIX B:
MECHANICAL AGING RESPONSE OF THE AL 6061-10 V/O AL_2O_3 PROCESSED WITH EXTRUSIONS AND DRAW/ANNEAL OPERATIONS.

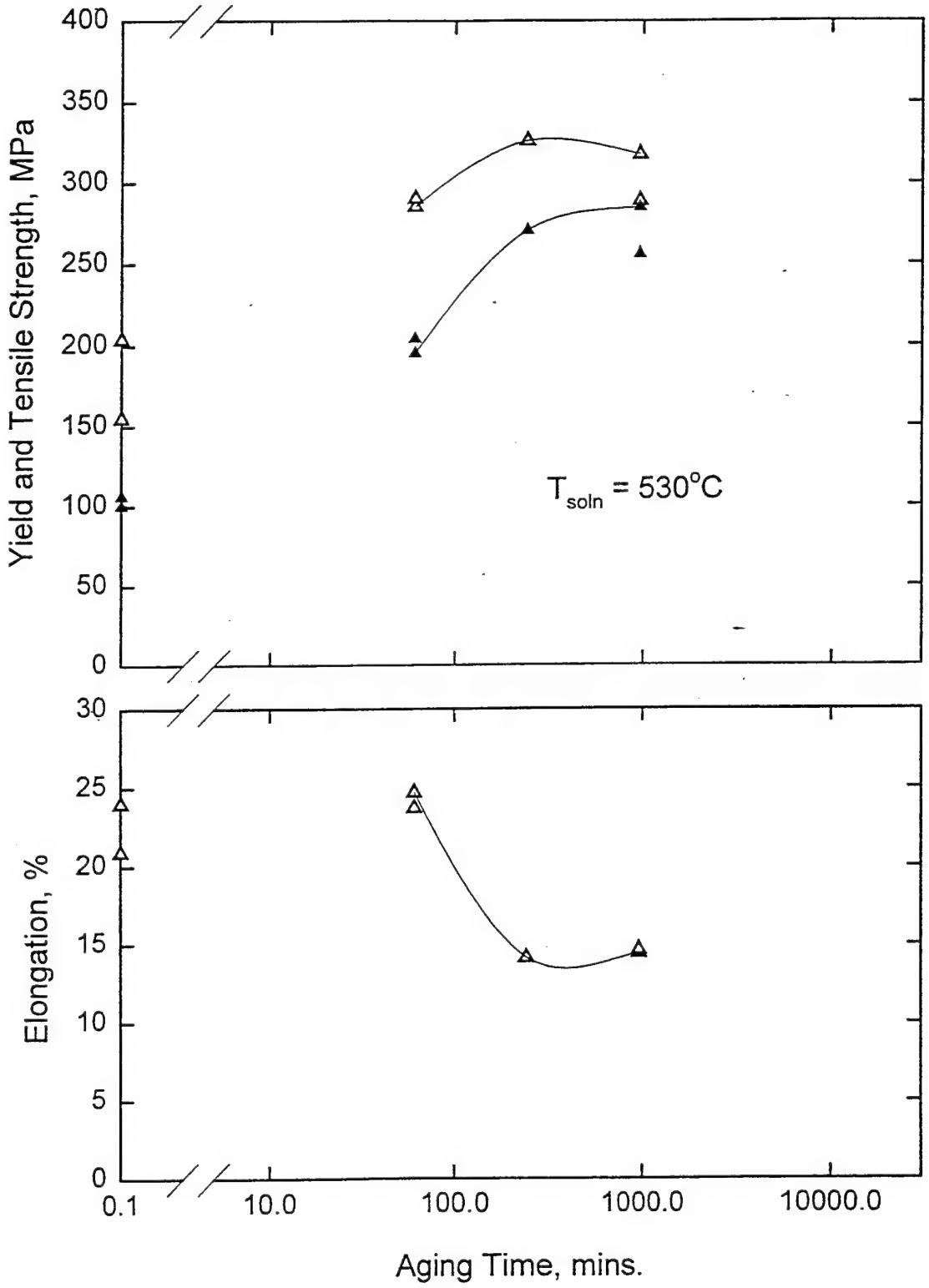

APPENDIX C:
MECHANICAL AGING RESPONSE OF THE AL 6061-20 V/O AL_2O_3 PROCESSED WITH EXTRUSIONS ONLY.

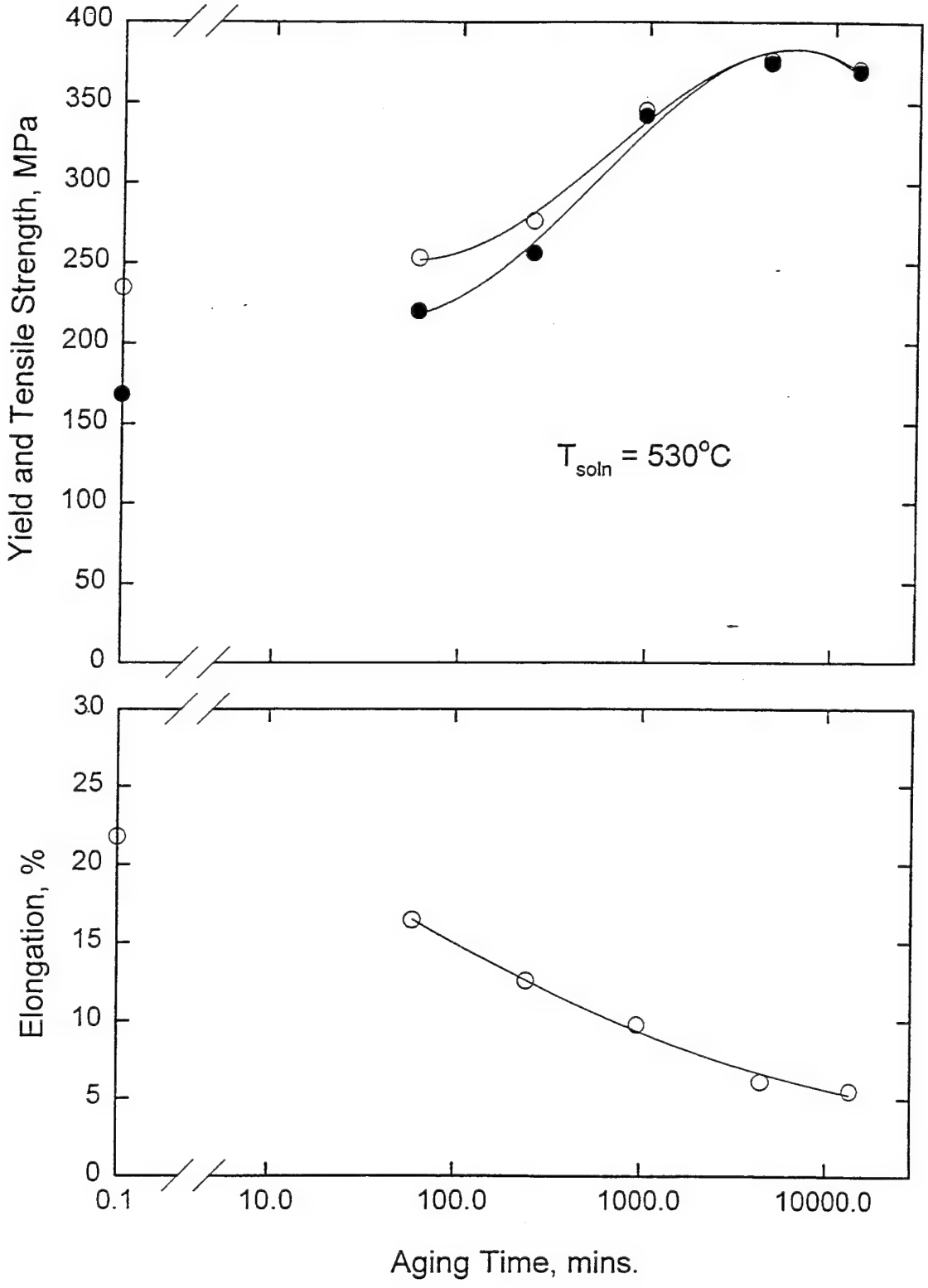

APPENDIX D:
MECHANICAL AGING RESPONSE OF THE AL 6061-20 V/O AL_2O_3 PROCESSED WITH EXTRUSIONS AND DRAW/ANNEAL OPERATIONS.

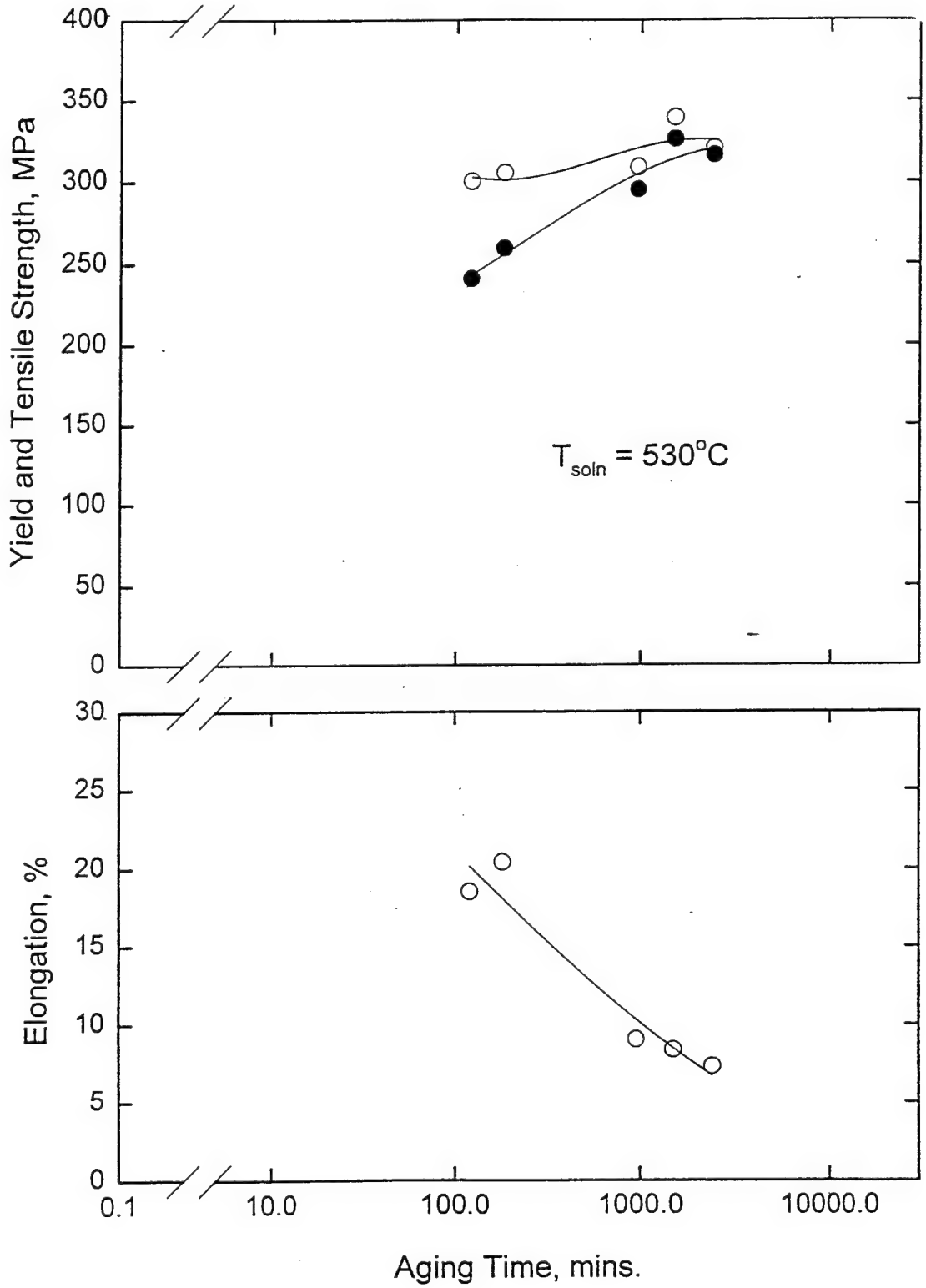

LIST OF REFERENCES

1. Hoyt, W. F., *The Effect of Thermomechanical Processing on Mechanical Properties of a Cast 6061 Aluminum Metal Matrix Composite*, Master's Thesis, Naval Postgraduate School, Monterey, California, December 1993.

2. Kalu, P. N. and McNelley, T. R., "Microstructural Refinement by Thermomechanical Treatment of a Cast and Extruded Al2O3 Composite", *Scripta Metallurgica et Materialia*, Pergamon Press, Vol. 25, pp.853-858, (1991).

3. McNelley, T. R. and Kalu, P. N., "The Effects of Thermomechanical Processing on the Ambient Temperature Properties and Aging Response of a 6061 Al-Al_2O_3 Composite", *Scripta Metallurgica et Materialia*, Pergamon Press, Vol. 25, pp.1041-1046, (1991).

4. McNelley, T. R. and Kalu, P. N., "Thermomechanical Processing and Ductility Enhancement of a 6061 Al-Al_2O_3 Metal Matrix Composite", *Advanced Synthesis of Engineered Structural Materials*, ASM International, Materials Park, Ohio (1992).

5. Schaefer, T. A., *Thermomechanical Processing and Ambient Temperature Properties of a 6061 Aluminum 10 Volume Percent Alumina Metal Matrix Composite*, Master's Thesis, Naval Postgraduate School, Monterey, California, March 1990.

6. Macri, P. D., *Processing Microstructure and Elevated Temperature Mechanical Properties of a 6061 Aluminum-Alumina Metal Matrix Composite*, Master's Thesis, Naval Postgraduate School, Monterey California, December 1990.

7. Magill, M. D., *The Influence of Thermomechanical Processing Parameters on the Matrix Composite Material*, Master's Thesis, Naval Postgraduate School, Monterey, California, December 1990.

8. Schauder, T. J., *The Elevated Temperature Behavior of a 10% Volume Al-Al_2O_3 Metal-Matrix Composite*, Master's Thesis, Naval Postgraduate School, Monterey, California, March 1992.

9. Eastwood, D. F.,*The Effect of Thermomechanical Processing Parameters on the Ambient Behavior of 10% Volume Al-Alumina*, Master's Thesis, Naval Postgraduate School, Monterey, California, March 1992.

10. Manfredi, M. S., *Computer Simulation of Random and Non-Random Second Phase Particle Distributions for Both Constant and Varying Particle Size*, Master's Thesis, Naval Postgraduate School, Monterey, California, September 1992.

11. Hunt, W. H., Richmond, O. and Young, R. D., in *6th International Conference of Composite Materials*, Vol. 2, Elsevier (1987).

12. Chawla, K. K., *Composite Materials: Science and Engineering*, Springer-Verlag (1987).

13. Schier, J. F. and Juergens, R. J., *Astronautics and Aeronautics*, Vol 44 (1983).

14. Clyne, T. W. and Withers, P. J., *An Introduction to Metal Matrix Composites*, Cambridge University Press (1993).

15. Hansen, N., *Dispersion Strengthened Aluminum Products- Manufacture, Structure and Mechanical Properties*, Riso National Laboratory, Denmark.

16. Chin, E. S. C., Beck, J. C., Huang, P. J., Wickman, H. A. and Biederman, R. R., *Thermomechanical Processing of Metal Matrix Composites for Ballistic Protection.*

17. McNelley, T. R., Crooks, R., Kalu, P. N. and Rogers, S. A., "Precipitation and Recrystallization During Processing of a Superplastic Al-10Mg-0.1Zr Alloy", *Materials Science and Engineering*, A166 pp.135-143 (1993).

18. Hales, S. J., McNelley, T. R. and McQueen, H. J., *Metallurgical Transactions*, Vol. 22, p.1037 (1991).

19. Hales, S. J. and McNelley, T. R , in *Proc. Symp. on Superplasticity in Aerospace*, TMS, Warrendale, Pennsylvania, p. 61 (1988).

20. Crooks, R, Hales, S. J. and McNelley, T. R., in *Superplasticity and Superplastic Forming*, TMS, Warrendale, Pennsylvania, p. 61 (1988).

21. McNelley, T. R. and Kalu, P. N., in *Proc. of Superplasticity in Advanced Materials*, JSRS, Osaka University, Osaka, Japan. p.413 (1991).

22. Hales, S. J., McNelley, T. R. and Crooks, R., in *Recrystallization '90, Proc. Int. Conf.*, TMS, Warrendale, Pennsylvania, p. 231 (1990).

23. Gorsuch, T. E., *The Roles of Strain and Reheating Interval in the Continuous Recrystallization During Thermomechanical Processing by Warm Rolling of an Al-Mg Alloy*, Master's Thesis, Naval Postgraduate School, Monterey, California, December 1989.

24. Rogers, S. A., *The Roles of Particles in Recrystallization of a Thermomechanically Processed Al-Mg Alloy*, Master's Thesis, Naval Postgraduate School, Monterey, California, September 1992.

25. Longenecker, F. W., *An Analysis of the Microstructure and Reinforcement Distribution of an Extruded Particle-Reinforced Al 6061-10 Volume Percent Al_2O_3 Metal Matrix Composite*, Master's Thesis, Naval Postgraduate School, Monterey, California, September 1993.

26. Selvaduray, G., Hickman, R., Quinn, D., Richard, D. and Rowland, D., "Relationship Between Microstructure and Physical Properties of Al_2O_3 and SiC Reinforced Aluminum Alloys", *Interfaces in Metal Ceramics Composites Conference*, The Minerals, Metals and Materials Society (1990).

27. Humphreys, F. J., Miller, W. S. and Djazeb, M. R., "Microstructural Development During Thermomechanical Processing of Particulate Metal-Matrix Composites", *Materials Science and Technology*, Vol. 6, pp. 1157-1166 (1990).

28. Shelton, D., Naval Postgraduate School, Monterey, California, Private Communication.

29. *Metals Handbook*, Ninth Edition, Vol. 4 Heat Treating, American Society for Metals, Metals Park, Ohio (1980).

30. Jeffrey, P. W. and Holcomb, S., "Extrusion of Particulate-Reinforced Aluminum Matrix Composites", in *ASM Conf. Proc. Fabrication of Particulates Reinforced Metal Composites*, ASM International (1990).

31. Peet, B. B., *Thermomechanical Processing of an Al Alloy 2519, and an Assessment of its Superplastic Response*, Master's Thesis, Naval Postgraduate School, Monterey, California, June 1995.

INITIAL DISTRIBUTION LIST

1. Defense Technical Information Center 2
   8725 John J. Kingman Rd., STE 0944
   Ft. Belvoir, VA 22060-6218

2. Library, Code 13 2
   Naval Postgraduate School
   Monterey, CA 93943-5101

3. Naval Engineering Curricular Office, Code 34 1
   Naval Postgraduate School
   Monterey, CA 93943-5100

4. Department Chairman, Code ME 1
   Department of Mechanical Engineering
   Naval Postgraduate School
   Monterey, CA 93943-5100

5. Dr. T. McNelley, Code ME/Mc 5
   Department of Mechanical Engineering
   Naval Postgraduate School
   Monterey, CA 93943-5100

6. LT Michael A. Ballou 2
   (Code 300)
   Commander Pearl Harbor Naval Shipyard
   401 Ave E Suite 24
   Pearl Harbor, HI 96860-5350